AD-A094 396 AIR FORCE INST OF TECH WRIGHT-PATTERSON AFB OH SCHOO--ETC F/G 20/5
MULTIPULSE LASER ANNEALING OF SELENIUM IMPLANTED GAAS.(U)
DEC 80 R A CONTRERAS
UNCLASSIFIED AFIT/GEO/PH/80D-5 NL

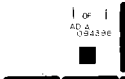

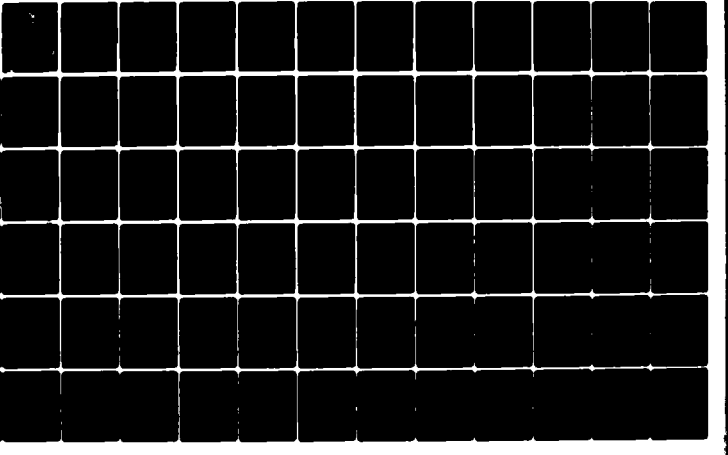

LEVEL II

AD A094396

UNITED STATES AIR FORCE
AIR UNIVERSITY
AIR FORCE INSTITUTE OF TECHNOLOGY
Wright-Patterson Air Force Base, Ohio

81 2 02 014

AFIT/GEO/PH/80D-5

II

0

APPROVED FOR PUBLIC RELEASE AFR 190-17. 14 JAN 1981

Fredric C Lynch

FREDRIC C. LYNCH, Major, USAF
Director of Public Affairs
Air Force Institute of Technology (ATC)
Wright-Patterson AFB, OH 45433

MULTIPULSE LASER ANNEALING OF SELENIUM IMPLANTED GaAs

Thesis

AFIT/GEO/PH/80D-5 Ricardo A. Contreras
Captain USAF

Approved for public release; distribution unlimited

AFIT/GEO/PH/80D-5

MULTIPULSE LASER ANNEALING OF SELENIUM IMPLANTED GaAs

THESIS

Presented to the Faculty of the School of Engineering
of the Air Force Institute of Technology
Air University (ATC)
In Partial Fulfillment of the
Requirements for the Degree of
Master of Science

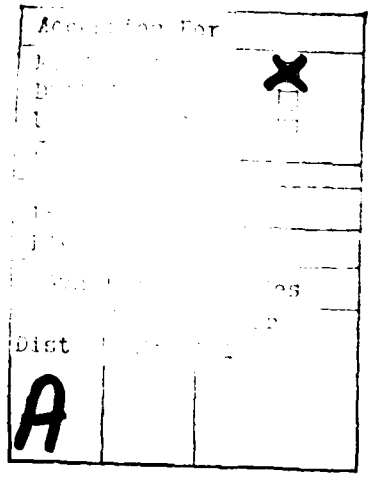

by

Ricardo A. Contreras
Captain USAF

Graduate Electrical Engineering

December 1980

Approved for public release; distribution unlimited

Preface

This thesis was a continuation of research which was begun by Lieutenants Kenneth Bradley and Bill Mullins. In particular, Lt. Mullins observed evidence from surface reflectivity measurements which seemed to indicate damaged crystalline layers were improved after irradiation by laser multipulsing. The results of my work indeed show this improvement of damaged crystalline material by use of multipulsing techniques.

There are several individuals who deserve a special note of my appreciation. Lt. Kenneth Bradley was very instrumental in assisting me in becoming familiar with the Neodymium YAG laser. Lt. Bill Mullins, who shared his experience with me concerning the UV reflectivity apparatus. A special thanks to Messrs. Jim Miskimen, George Gergal, Ron Gabriel, and Bob Hendricks for their support in all matters concerning laboratory equipment, modifications and materials. Mr. David Walsh, who in the early days of the experiment, assisted me in the terrible times of making aluminum coated reflective surfaces.

Of course, this thesis would never have been possible without the expert guidance and experience of two particular professors. Dr. Theodore Luke, my thesis advisor, who readily made available his support and highly technical assistance. Also, Dr. Robert Hengehold, whose constant advice and expertise in the reflectivity equipment proved to be invaluable.

I would also like to thank Dr. Y.S. Park of the Air Force Avionics Laboratory (AFWAL) for his support in providing me with all of the GaAs substrates. Despite his very busy schedule, Dr. Park was the primary reason all substrates were made available to me in a most expeditious manner.

My final words of thanks and praise go to my lovely wife, Kathy, who supported me with words of encouragement, and my three children, Richard, Michael and Jacqueline, all of whom gave up countless weekends and evenings with me while I worked the long hours in the laboratory. Their continued support and patience were almost magical. I thank each and every one of them with my love.

Contents

List of Figures

List of Tables

Abstract

GaAs implanted with 120 keV Se at a fluence of 10^{14} ions/cm^2 was laser annealed using .53μ energy from a Q-switched, frequency doubled, Neodymium:YAG laser. The substrates were irradiated in air by either a single pulse or multipulse with an average energy density of 300 mj/cm^2 per pulse. The pulse width (FWHM) was 15 ns. Optical reflectivity in the ultraviolet spectrum of 210 nm to 380 nm was used to evaluate the crystalline structure. The relative crystalline damage versus depth profile was obtained and compared to that of an as-implanted sample. The depth profiling was accomplished using a chemical etch. Implanted samples annealed at 1, 2, 4, 8, and 12 pulses all showed a dramatic reduction of damage as compared to the as-implanted sample. However, the results of the two pulse anneal show the highest degree of recrystallization approaching that of a virgin sample.

MULTIPULSE LASER ANNEALING OF SELENIUM IMPLANTED GaAs

I. Introduction

Semiconducting materials are of extreme importance to the Air Force. Silicon, germanium, and gallium arsenide, to name a few, are used in the fabrication of optical detectors, solar cells, microelectronics, and in high speed integrated circuits. In the near future, a real possibility exists for the development of large scale integrated circuit microprocessors with as much as one million devices on a single, 400 micrometer squared chip. Some of these same materials are also used in the manufacturing of critical optical components such as windows, lenses, and modulators. However, the full potential is realized after the materials have been implanted with dopant impurities forming n-type, p-type, or p-n junction layers.

Some of the more conventional techniques for the impurity addition to materials or substrates are the following: 1) melt doping during crystal growth; 2) thermal diffusion; 3) alloying of the desired impurity into the substrate; and 4) ion implantation. Each of these methods have their advantages and disadvantages with respect to each other. However, ion implantation has proven to be particularly advantageous in the following areas of concern: 1) nearly any impurity

can be introduced to a variety of substrates in precise amounts; 2) doping profiles can be controlled in three dimensions by modulating the energy, current, and the position of the ion beam; and 3) the process has the capability of introducing a pure dopant into the substrate (Ref 1).

The ion implantation process involves the use of an energetic ion beam to introduce ions into a substrate. During this ion bombardment process, the substrate is losing some of its own ions due to sputtering and, at the same time, retaining some of the incident ions. Consequently, a damaged region within the crystalline struction is being formed. This simply means the crystal lattice structure of the substrate has been disrupted, leaving dislocations and dislocation loops, stacking faults and clusters of point defects (Ref 2). Also, the implanted ions have not settled into substitutional lattice sites (Ref 3). Therefore, a mechanism for the repair of the crystal damage and which enhances substitutionality is required.

The repair mechanism is referred to as annealing. Annealing can remove defects within the ion implanted sample by causing the sample to recrystallize and, at the same time, help the impurity atoms relocate to substitutional sites. Some methods of annealing are: 1) furnace annealing, the process of heating the ion implanted samples to high temperatures in an oven for typically one hour; 2) pulsed electron beams, e-beam propagation from a cathode to an anode which impacts upon the material to be annealed; and 3) laser

annealing, which consists of irradiating the ion implanted substrate with a continuous wave or single pulse of intense laser radiation (Ref 4).

Laser annealing is the repair mechanism on which this study focuses its attention. Specifically, in the case of GaAs, is it possible to anneal damaged crystal regions due to ion implantation using a short, single pulsed or multi-pulsed frequency doubled Neodymium:YAG laser? Recently, several experiments on pulsed and continuous wave (CW) laser annealing of implanted GaAs substrates have shown promising results (Refs 5 & 6). Tellurium implanted GaAs samples irradiated with a Q-switched ruby laser with a 12 nsec pulse duration and an energy level of 1.5 J/cm^2 per pulse has shown significant crystal regrowth of the amorphous region (Ref 7). Mullins (Ref 8) studied the effects of laser annealing by using optical reflectivity spectra. He found that the optical reflectivity spectra of irradiated GaAs substrates implanted with 120 keV Te at a fluence of 10^{14} ions/cm^2 returned to that of the unimplanted substrates. The implanted GaAs was irradiated with a single pulsed, 30 nsec, ruby laser at a wavelength of 694.0 nanometers and various energy density levels. Mullins used a damage coefficient, D (Ref 9), in order to measure changes in the substrate. From this approach, he concluded that an adequate change in D corresponded to a substantial repair of the damaged crystalline surface.

The question arises whether, indeed, epitaxial regrowth has occurred as a direct result of laser irradiation. In

epitaxial regrowth, the depth of melt must be deep enough to overlap into the single crystal region of the GaAs, hence past the amorphous/crystalline interface. Thus, the single crystal acts as the seed for the regrowth of the crystalline lattice structure. Using D, the damage coefficient derived from the optical reflectivity of the surface, and a surface etching technique, a relationship between D and the depth can be established. This may yield the depth of melt information required and, to a first order measurement, evidence as to whether single crystalline material was formed in the implanted region.

The D versus depth profile after a single pulse of laser energy will exhibit a particular profile. This profile, of course, will vary depending on the following laser and sub strate parameters: 1) laser type; 2) Q-switched or continuous wave; 3) wavelength; 4) pulse length; 5) spatial energy distribution; 6) substrate temperature; 7) implant species; 8) implant fluence; and 9) implant temperature. Thus a variance of one or a combination of the parameters will effect the profile.

The purpose of this study is to establish a multi-pulsing technique at some ideal energy density level in order to determine whether the D versus depth profile for a single pulse of laser energy is improved. It is hope that optimum laser pulse parameters can be recommended which, in further studies, will lead to a successful laser annealing--i.e. elimination of defects, high electrical activation, and

carrier mobility.

The frequency doubled Neodymium:YAG laser will be used to provide the .53μ pulsed energy. The samples to be examined are Se implanted GaAs.

II. Theory

Laser Annealing

Ion implanted crystals will normally contain a great deal of damage in the as-implanted state. This damage is a direct result of the ion bombardment process upon the crystal lattice. The damage must be annealed in such a way that 1) implanted ions will be incorporated into electrically active (usually substitutional) sites in the crystal lattice and 2) residual defects are reduced to a level where carrier mobilities and lifetimes are not degraded (Ref 2). Hence, successful laser annealing is an effect which produces characteristics in a sample comparable to, or better than, thermal annealing.

There are two basic techniques for laser annealing: liquid-phase epitaxial regrowth and solid-phase epitaxial regrowth. Liquid-phase epitaxial regrowth utilizes pulsed lasers, with their high energy output, to raise the temperatures of the material above its melting point. After the surface temperature rises past the point of melt, the "melt front" moves inward and reaches its maximum depth in slightly more time than the duration of the pulse. If the entire amorphous layer is melted, epitaxial regrowth occurs with the underlying substrate acting as a seed (Ref 10).

Solid-phase epitaxial regrowth occurs in the case where the implanted layer does not melt. Bell Labs has performed research using an argon-ion laser to raise the

temperature of Si to between 900°C and 1300°C, below the 1400°C melting point. Krypton and argon, the predominate lasers, were operated in the continuous wave (CW) mode, usually in conjunction with a scanning apparatus. Bell Labs reported the prime advantage of this type of epitaxial regrowth was the fact the dopant profile was narrower than that possible with thermal annealing (Ref 3).

Most laser work has been performed with nanosecond laser pulses. Khaibullin, et al. (Ref 11) have stated the fast process, 1 to 100 ns pulse widths, yields several interesting effects. Besides thermal, there are other effects such as photoionization, impact wave, and possibly powerful light fields. They also reported that for a high concentration of impurities, the limit of solubility of the impurities in silicon can be exceeded.

In the annealing of GaAs, the surface has shown an extreme sensitivity to heat. Evidence of Ga-rich surfaces after annealing has been reported (Refs 12 & 13). The capping of the sample prior to annealing is one method used to control the loss of the As. This problem can also be controlled by the shortening of the pulse widths. Uncapped GaAs, when annealed with a one nanosecond pulse, has a smaller concentration of Ga on the surface as compared to pulse widths of one millesecond. Bell Labs reported that good crystallinity and minimal loss of As for the nanosecond pulse region could be obtained. They also stated that the optimum for melt time was dependent upon concentration of implanted impurities (Ref 12).

Several parameters effect the laser annealing process: the concentration of the implanted impurities, the wavelength of the annealing laser, the substrate material, and the energy density used to anneal the sample are but a few. However, two of these parameters seem to have the greatest impact. The fundamental wavelength of the laser energy and the actual energy density seem to cause the most radical changes in the physical or electrical properties of the material (Refs 11, 14, 15 & 16). At low energy densities no changes occurred, but at high energy densities, visual damage such as craters, microcracks, and cavities in the surface began to appear. However, from report to report, there was a discrepancy in the energy density needed to produce the damage. This discrepancy was probably due to the method used to detect the damage and in the definition of the damage.

In the case of GaAs irradiated by ruby lasers, both Mullins (Ref 8) and Bradley (Ref 17) reported that the energy density which seemed to cause minimal surface effects, yet showed evidence of recrystallization via optical reflectivity measurements, was at the level of .35 J/cm^2. The laser annealing was performed using a Q-switched ruby laser with a 30 nsec pulse width. The GaAs samples were implanted with 120 keV Te at a fluence of 10^{14} $ions/cm^2$. Campisano, et al. (Ref 18), have reported the following results: with a ruby laser pulse of 50 ns, GaAs wafers implanted with 400 keV Te^+ ions at a fluence of 10^{15} $ions/cm^2$ exhibited a threshold energy density of 1.0 J/cm^2 above which the layer regrows epitaxially. Below

the threshold, the layer is polycrystalline; the grain size increasing as the energy density approaches threshold. Recrystallization was evaluated using backscattering spectrometry and transmission electron microscopy.

Besides energy density, the wavelength of the laser has a major effect on the laser interaction with the substrate. As reported by Mason (Ref 6), the absorption coefficient (α) for pure GaAs is 2×10^4 cm^{-1} at the ruby wavelength, $\lambda = 6943\text{Å}$. After implantation, the absorption will increase due to the damage in the implant layer, but the degree of change is unknown. Also, unknown are the effects of the implantation at the air-implant layer interface, as well as the implant layer substrate interface and the refractive index at these boundaries. These parameters must be known in order to yield information on the surface which reaches the implant layer through the interface, and how much of this energy is absorbed by that layer.

The absorption coefficient will change within the material depending upon the degree of damage due to ion implantation. However, the exact degree of change of α is not well known. For the sake of argument, it is assumed that the absorption increases as the degree of damage increases. Thus, at small implant energies, roughly 20 keV, the degree of damage within the surface is relatively shallow. This condition may yield an α which is somewhat similar to that of a pure substrate. For large implantation energies, about 400 keV, the degree of damage is increased along with its implant profile

(Ref 19). This may yield an absorption coefficient which is a substantial increase over that of the pure substrate. The effect on the laser energy can, therefore, be detrimental since an energy decay to a small fraction of its surface value may occur by the time the pulse wave reaches the implant-substrate boundary (Ref 6).

In the case of the .53μ wavelength of the frequency doubled Neodymium:YAG laser, the absorption coefficient for pure GaAs is calculated to be $\alpha = 7.82 \times 10^4$ cm^{-1}, where

$$\alpha = \frac{4\pi k}{\lambda} \qquad (1)$$

and k, extinction coefficient = .33 (Ref 19).

This value corresponds with Fig 1 which shows the absorption coefficient dependence on photon energy. The energy gap is the energy below which the absorption coefficient is $\gtrsim 1$ for a given material. Figure 1 indicates a drastic increase in the α as the energy gap is exceeded. Thus, in the case of the .53μ laser wavelength, the photon energy is 2.34 eV, which is much greater than the energy gap of GaAs, 1.43 eV. This results in a large absorption coefficient at the .53μ wavelength for GaAs.

In the case of GaAs implanted with 120 keV selenium to a fluence of 10^{14} ions/cm^2, the question remains as to how much will the absorption coefficient change with respect to the .53μ laser energy. In theory, the change in α can be assumed to be minimal since the fluence and implant energy level of the selenium is not drastically large. Thus, the

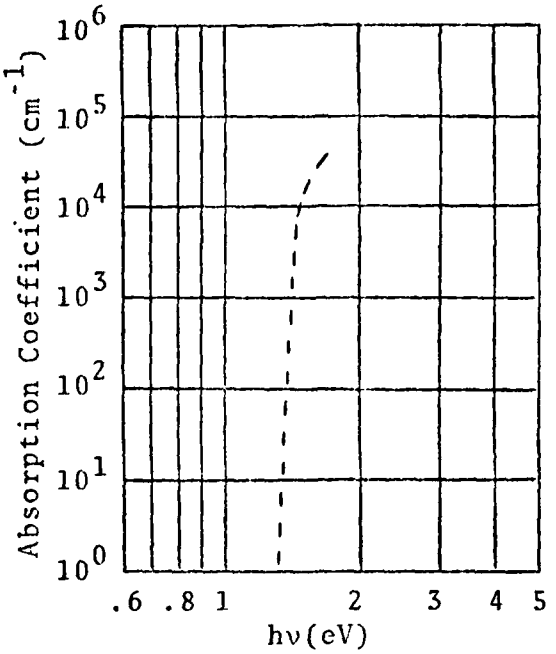

Fig 1. Absorption Coefficient Dependence on Photon Energy. Energy Gaps for GaAs at 300°k and 66°k [Ref 19:54]

depth of penetration of the .53μ energy should be sufficient to penetrate through to the implant-substrate boundary in order for liquid-phase epitaxial recrystallization to occur.

As a baseline for comparison, Figure 2 can be used as an estimate for depth of penetration of the .53μ energy. This figure yields an expected depth of penetration with respect to the ratio of the reflected intensity over the incident intensity. The theoretical curve is based on $\alpha = 7.82 \times 10^{+4}$ cm^{-1} and the assumption that the α was not radically changed by the implant. From the curve, it can be assumed that ample energy within the pulse will be available so long as I_r/I_o at the surface is not smaller than .6. The curve is derived from the Beers Law relationship where

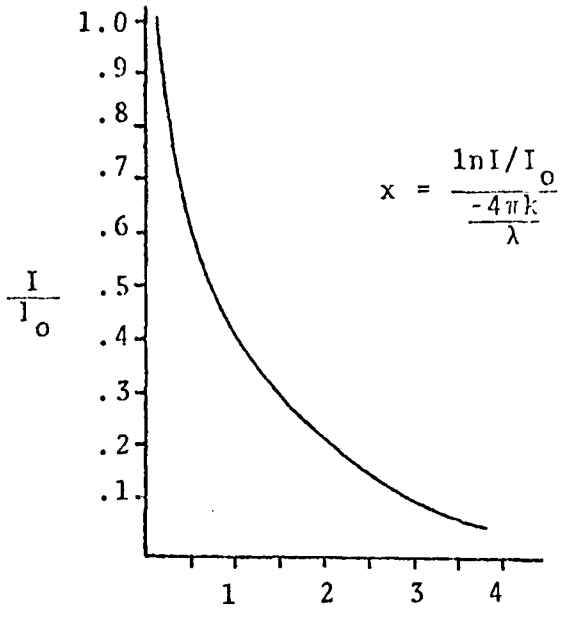

Fig 2. Theoretical Curve Showing the Depth of Penetration of .53μ Energy for Pure GaAs

$$I = I_o e^{-\alpha x} \tag{2}$$

thus

$$\ln I/I_o = -\alpha x \tag{3}$$

and

$$x = \frac{\ln I/I_o}{\frac{-4\pi k}{\lambda}} \tag{4}$$

x is the depth of penetration; λ, the wavelength of the incident energy I_o.

It is not known for certain how deep the .53μ energy will penetrate into the implanted region. Absorption coefficient data seem to indicate a good possibility that the .53μ wavelength of the pulse will permit energy to reach the implant-crystalline boundary layer in order to promote complete

amorphous melting. Using the multipulsing technique, a repetition of pulses which do not cause surface damage, each pulse may see succeeding optimum crystalline structure, thus enhancing the "melt front" to reach the crystalline region. Hence, liquid-phase epitaxy can occur since the underlying substrate can act as a seed for the crystalline growth.

Ultraviolet Reflectivity

The reflectivity, R, of a substance is defined as the ratio of the reflected I_r to the incident I_o intensities from a surface such that:

$$R \equiv I_r/I_o \tag{5}$$

The Fresnel equations for the reflectivity for non-conducting media has the form

$$R_{\perp} = |r_{\perp}|^2 = \left|\frac{n_2\cos\theta_i - n_1\cos\theta_t}{n_2\cos\theta_i + n_1\cos\theta_t}\right|^2 \tag{6}$$

and

$$R_{\parallel} = |r_{\parallel}|^2 = \left|\frac{n_1\cos\theta_i - n_2\cos\theta_t}{n_1\cos\theta_i + n_2\cos\theta_t}\right|^2 \tag{7}$$

θ_i and θ_t are the angle of incidence and refraction; n_2 and n_1 are the index of refraction for the absorbing and surrounding mediums. The $\parallel$ and $\perp$ refer to the parallel and perpendicular components to the plane of incidence, respectively.

Mullins (Ref 8) showed Eqs (6) and (7) rederived so that they include the complex index of refraction for a conducting media. Thus, Eqs (6) and (7) become:

$$R = \left|\frac{(n+ik)\cos\theta_i - n_1\cos\theta_t}{(n+ik)\cos\theta_i + n_1\cos\theta_t}\right|^2 \qquad (8)$$

and

$$R = \left|\frac{n_1\cos\theta_i - (n+ik)\cos\theta_t}{n_1\cos\theta_i + (n+ik)\cos\theta_t}\right|^2$$

and θ_i is related to θ_t by Snell's law; k is the extinction coefficient.

In a conducting medium, since $\hat{n}$, the complex index of refraction, is a function of ω, then R is also a function of ω (Ref 21). This functional relationship of $\hat{n} = \hat{n}(\omega)$ can be better understood by studying the correlation between the fundamental electrical properties of and the optical dispersion in a conducting media. Dispersion, or a dispersive medium, occurs when light passes through a medium where the index of refraction (hence the phase velocity) is a function of frequency. This arises from the fact that the phase velocity and group velocity may differ only when the phase velocity is a function of the frequency, thus only when ω itself is other than a linear function of the propagation constant of a wave train (Ref 22).

Dispersion in a semiconductor arises from bound and free electrons. The free electrons contribute primarily to the long wavelength absorption bands while the bound electrons contribute to the absorption at energies higher than the fundamental absorption edge, the region of interest in this experiment. The motion of the bound electron is described by the classical Lorentz oscillator. The complex dielectric

function, $\hat{\varepsilon}$, is treated in the study in order to yield the total effect of a crystal containing j different oscillators, f_j in number, with characteristic constants ω_j and γ_j. Thus, the total effect is the sum of the individual contributors:

$$\hat{\varepsilon} = 1 + \frac{4\pi e^2}{m} \sum_j \frac{f_j N_j}{(\omega_j - \omega^2) - i\gamma_j \omega} \qquad (10)$$

$$\sum_j N_j = N \qquad \text{[Ref 8]}$$

A further study will show that as the extinction coefficient, k, increases, so does the absorption and reflectivity (Ref 21). As the electrons start to absorb the incident radiation, they are excited, start a harmonic resonance, and re-emit the incident radiation. Thus, the reflectance reaches a peak value near the resonant frequency ω_j. If f_j is not the same for all oscillators, some frequencies will have stronger absorption and reflectance than others, thus a reflectance spectrum is produced.

Optical reflectivity is a good tool to measure the regrowth of the amorphous layers. This is due to the fact that the periodic internal field of the crystal is responsible for the band structure and reflectivity spectrum. During the ion implantation process, the crystal lattice structure, or long range order, is ruined to a level which is directly dependent on the dosage of the ion. This, in turn, has a direct effect upon the reflectivity spectrum, $R(\omega)$, of the crystal surface. At low dosages, the $R(\omega)$ which may still be present can be attributed to smaller areas of crystalline

order. Eventually, as the implantation dosage increases, all semblance of the $R(\omega)$ of the original surface is overwhelmed by the $R(\omega)$ of the now dominant amorphous surface. The annealing process attempts to return the surface back to the $R(\omega)$ which existed prior to the ion implantation process. Therefore, the annealed surface is now composed of a crystalline structure possessing a long range order. In theory, this re-established long range order may yield an $R(\omega)$ which is similar to that which existed prior to the ion implantation process.

Miyao, et al. (Ref 9) described a system by which the peak and valley differences of the $R(\omega)$ curve could be used to measure the crystallinity. This measurement would be independent of surface effects such as an oxide layer buildup due to atmospheric effects. A damage criterion, D, is established for which $D = 0$ is for a crystalline sample, and $D = 1$ is for an amorphous sample.

The damage to the surface of the crystal is given by:

$$D = \frac{(R_1^c - R_1^c)/R_2^c - (R_1^s - R_2^s)/R_2^s}{(R_1^c - R_2^c)/R^c - (R_1^a - R_2^a)/R_2^a} \qquad (11)$$

where R_1 and R_2 are the reflectance at the peak and the valley of the crystal, respectively. The superscripts, c and a, represent the standard samples for the crystalline and amorphous layers, and s represents the sample under investigation. In the experiment, the GaAs R_1 and R_2 were established at 247nm and 335nm, respectively.

The depth of penetration of the UV intensity can be described by Eq (4). At the wavelengths of R_1 and R_2, the average depth was calculated to be 30Å and 130Å, respectively. This calculation is based on the extinction coefficient, k, at R_1 to be equal to k = 3.279, and at R_2, a k = 1.88 (Ref 19). Thus, the crystallinity measured by Eq (11) is only for the first few crystal layers to a depth of 130Å.

A bracketed energy density, level E_d, for the laser annealing pulse can be experimentally derived from the use of the D parameter. As E_d approaches an optimum value (optimum with respect to energy density only) which yields the best level of damage repair, a minimum value for D approaching D = 0 is obtained. As the E_d level is increased or decreased, the D parameter should vary in such a manner that the best E_d level can be bracketed, or optimized, with respect to the minimum D obtained, or conversely, with respect to the best level of repair of the damage crystalline surface. Mullins (Ref 8) found in annealing Te implanted GaAs using a Q-switched ruby laser, that the best one shot E_d level was .35 J/cm^2. He stated that at this level the R(ω) spectrum of the annealed sample approached that of a virgin crystalline sample.

The optimum E_d level for the .53μ energy of the Neodymium:YAG laser is expected to be similar to that of the ruby level as found by Mullins. In theory, a multipulsing technique utilizing the .53μ E_d level may improve the extent of the crystalline repair. The R(ω) spectrum at various

etched levels should yield a D parameter at each level which will, in essence, provide a D versus depth profile for substrates annealed by multipulsing at a pulse whose E_d is the established optimum level.

III. Experiment

Laser Annealing

The laser used in the experiment was the Quantel YG 482CM Neodymium:YAG system. It is a complete and independent system which operates in a purely TEM_{oo} mode producing a pseudo-gaussian beam shape. The system is built around three YAG heads operating at a maximum of 5 pps, an electro-optical Q-switch, and a frequency doubler. All laser irradiation and annealing was performed in ambient air.

The frequency doubler device is composed of a 12mm x 12mm x 35mm type 1 crystal of deuterated KD*P, installed in an index-matching liquid cell. The windows are AR coated for minimum loss. Also, the frequency doubler is temperature controlled ($0 \pm .1°C$) in order to provide better stability.

The electro-optical Q-switch contains a longitudinal field Pockels cell with a KD*P crystal (AR coated windows), a high quality AR coated Glan Taylor polarizer, and an internal solid state power supply and fast electronics board and switching circuit.

The oscillator and amplifier rate is variable from single shot to 5 pps. The diffraction limited beam has a rated beam divergence of .6 milliradians full angle (for 90% of the energy). The pulse duration (FWHM) was found to be 15 ns with no detectable change when varying the output of

the .53μ energy from 80 to 200 millijoules measured at the location of the sample.

The experimental arrangement is shown in Fig 3. All annealing was performed in ambient air. Two dichroic beamsplitters, positioned at a 45° incidence, were used to separate the 1.06μ wavelength and the .53μ wavelength emanating from the frequency doubler. The .53μ beam from the second dichroic was then directed onto the sample. The sample was located approximately 109 cm from the second dichroic. The HeNe laser was used solely for substrate alignment with respect to the beam spot location. During actual annealing, the HeNe laser was turned off.

The annealing of a sample was performed using a single pulse of energy in the manual Q-switched mode. It was found during equipment preparations and alignment that from pulse to pulse, the energy of the .53μ light could vary by as much as 10%. Therefore, a method to determine the actual energy in each pulse during laser annealing was developed.

Two methods for measuring the actual energy density in a single pulse were considered. One consisted of placing a glass microscopic slide at a 45° incidence between the second dichroic beamsplitter and the sample location. The EG&G radiometer was positioned so as to receive the reflected .53μ light from the microscopic surface. However, upon close examination of the image of the beam spot at the sample location, it was found that interference fringes within the .53μ spot image was created by the glass slide. This interference

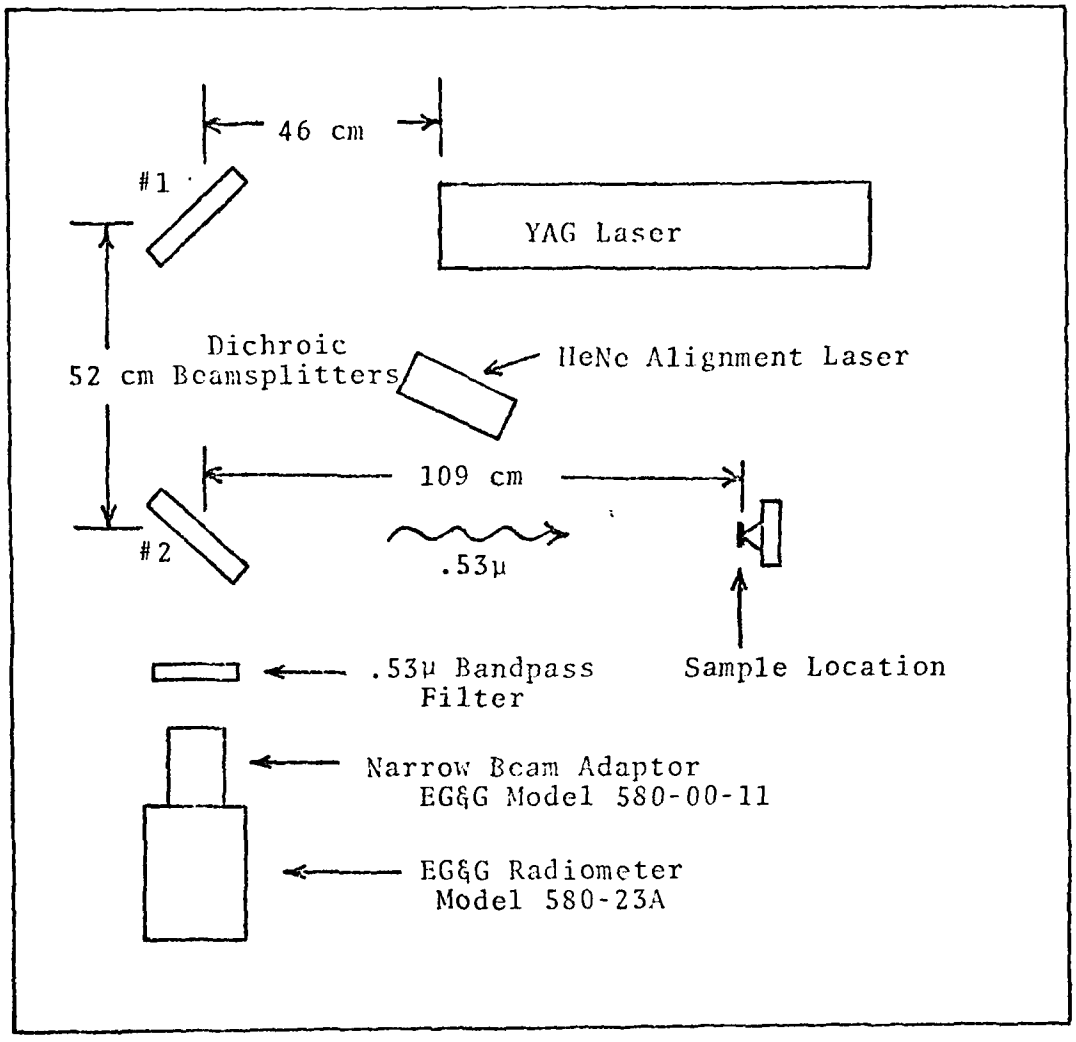

Fig 3. Equipment Configuration for Laser Annealing

was due to the multipath effect of the two surfaces of the slide. Other glass pieces of various substances were examined in order to decrease the reflectance and the incidence angle, but none proved to be feasible since in all cases the interference fringes were still visible. Therefore, this method was abandoned in lieu of repositioning the EG&G in a position off the transmitted side of the second dichroic beamsplitter, Fig. 1.

The repositioning of the EG&G behind the second beamsplitter required that the EG&G be calibrated for this station. This was accomplished by using a Scientech detector placed at the location of the sample. A single Q-switched pulse of energy was manually triggered in order to irradiate both the Scientech and the EG&G simultaneously with .53μ energy. The .53μ energy transmitted through the beamsplitter was extremely small in total charge as compared to the .53μ energy received by the Scientech. However, the EG&G coupled with a narrow beam adaptor more than easily handled the small charge ranges of 10^{-10} coulombs. A .53μ filter was placed between the second dichroic and the EG&G in order to filter out any residual 1.06μ light. The output of the laser was then varied in order to yield an energy versus charge functional relationship between the Scientech and the EG&G. This function was standard throughout the experiment since it was only .53μ light which both detectors were being irradiated by. Thus, the tuning of the KD*P frequency doubling crystal did not effect the calibration since only .53μ light established the

reference. This calibration procedure was used to establish the average energy density per pulse measured real time.

The average energy density measurement was based on the calibration procedure of the previous paragraph. One modification was made in order to account for the actual spot size. A circular aperture with a diameter of .56 cm was placed over the Scientech and positioned within the center of the beam spot image. The image was detected using Kodak photographic paper, Type 1895, which had been exposed to light more than 24 hours. The Scientech located at the position of the sample, along with the EG&G off the second dichroic, provided a calibration of the EG&G which also considered energy density. Thus, during actual annealing, the only detector used was the EG&G which had remained stationary behind the second dichroic after completion of the calibration procedure. The Scientech was removed since it blocked the irradiation of the substrate. As the sample was irradiated during annealing, the EG&G would measure, real time, the actual charge within the .53μ pulse. The charge value, in coulombs, would then be converted to an energy value, in joules, via the calibration chart, Fig. 4. The energy value from the chart then yields an average energy density value by simply dividing this value by the area of the aperture which had been placed in front of the Scientech detector during the calibration. Thus directly, the average energy density of the pulse for the .53μ light was measured via the charge, in coulombs, detected by the EG&G stationed behind the second dichroic during the annealing

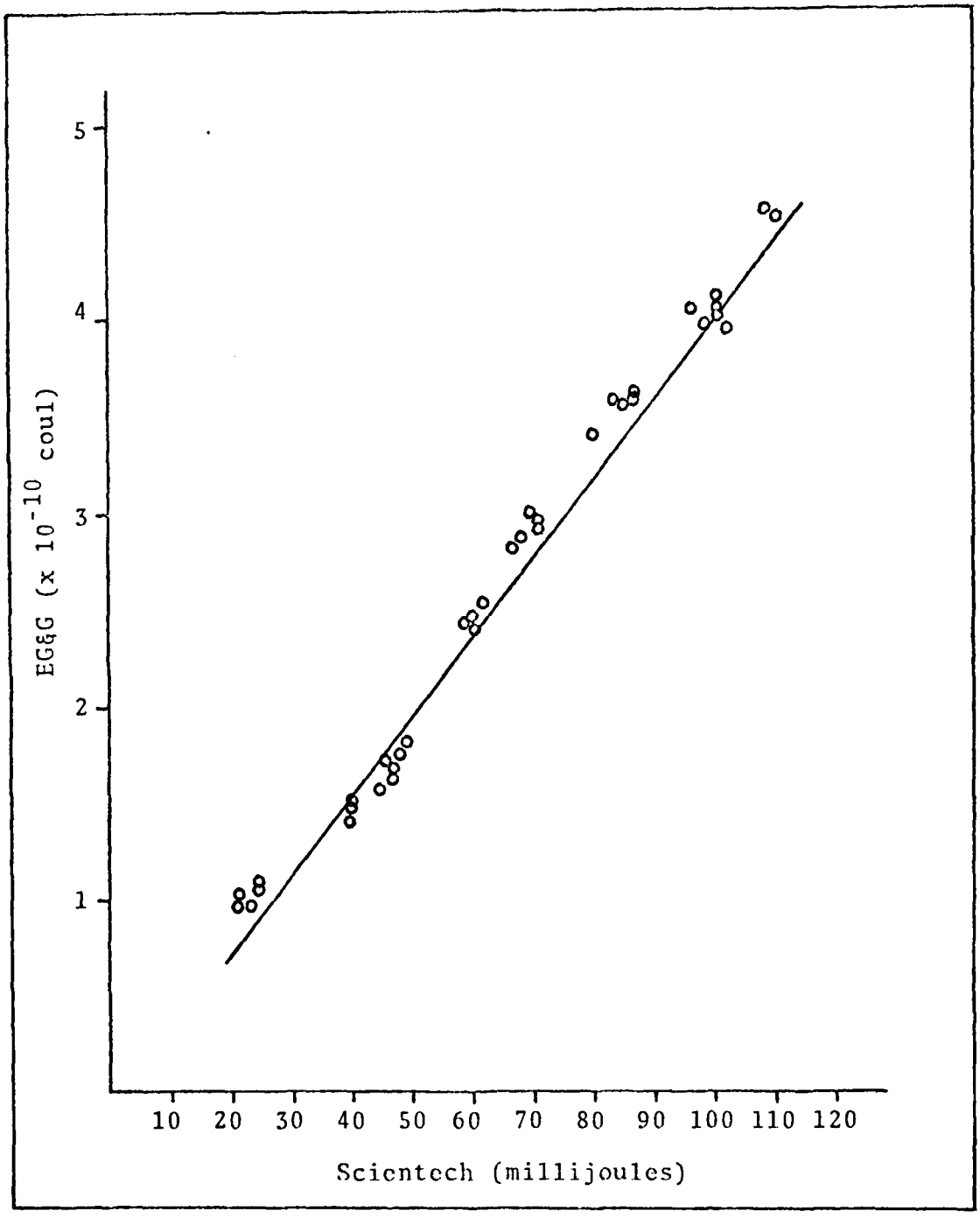

Fig 4. Calibration of EG&G Using Scientech Detector With .56 cm Circular Aperture

procedure.

The purpose of using an aperture of .56 cm during the calibration of the EG&G was twofold. First, the diameter size was conveniently chosen so as to provide an area which encompassed on the average, 98% of the total area of the substrates being irradiated. The GaAs substrates were nominally .5 cm x .5 cm cuts from a standard wafer. Thus, irradiation which overlapped the substrate during annealing was not important since the calibration procedure had negated this overlap. Secondly, the spatial energy distribution was found to be pseudo-gaussian, Fig 5. Thus, on the average, 85% of the energy was encompassed by the aperture. The pseudo-gaussian profile of the spatial energy distribution did not change significantly between the various energy density levels at which annealing was performed. Hence, for each pulse, the actual average energy density of the .53μ light was detected by the calibrated charge reading from the EG&G detector.

Laser Annealing Procedure

Each day before the laser annealing process was performed, the laser was tuned to yield maximum .53μ energy at the location of the sample station. The beam spot was also examined for its burn pattern using the Kodak photographic paper, Type 1895, to ensure the spatial distribution had not changed in an obvious manner.

Just prior to annealing, each sample was HF cleaned, then rinsed in distilled water to de-emphasize possible surface

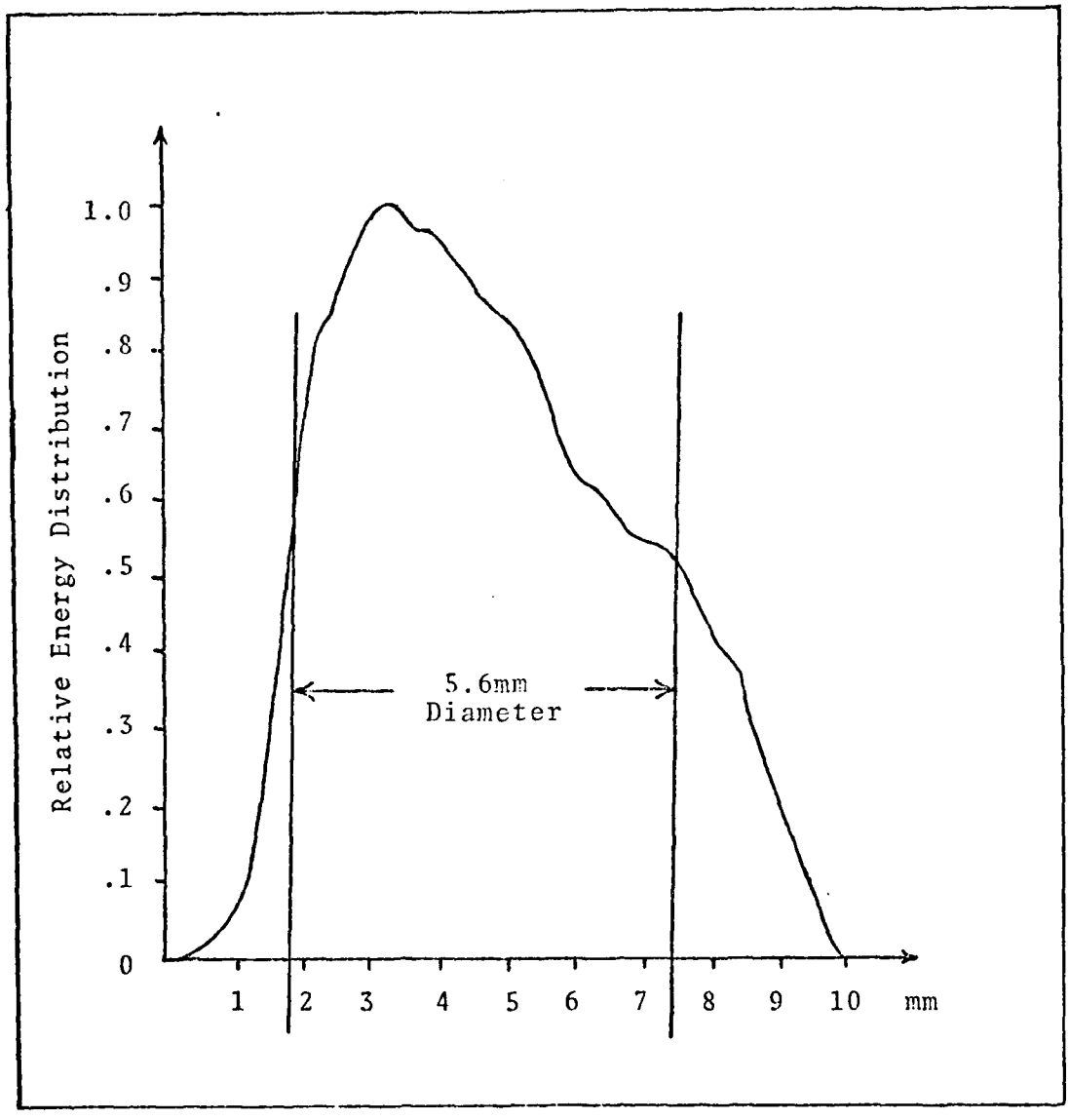

Fig 5. Spatial Energy Distribution

effects. The virgin GaAs and the implanted GaAs were all prepared in the same manner. Mullins (Ref 8) found that within a change of .1, D was insensitive to surface films. Also, he had concluded that the surface film on GaAs was not greatly affected by changes in the energy density of the annealing beam. Results obtained in this report substantiated this particular conclusion by Mullins.

The actual annealing process was performed using the HeNe laser for sample alignment on the center of the .53μ beam spot, and the EG&G radiometer for energy density measurements. The energy density level was dialed using the kilovolt level power supplies of the laser amplifiers. A block of wood was placed in front of the sample, while the laser was single pulsed test fired in order to ensure the proper energy density level was obtained on the EG&G radiometer. Once the proper energy density level was achieved, the block of wood was removed and the sample was irradiated with a single pulse. After irradiation, the sample was immediately placed within its storage container and annotated for actual energy density level it received.

The multipulse annealing was performed in the same manner. However, it was found that annealing energy densities were more consistent when the laser was fired for several pulses at 1 Hz, then switched to the manual mode of single pulse firing. This procedure seemed to compensate for possible heating effects of the rods by the flash lamps, whereas in the single mode, the rods were in various stages of heat profiles.

Thus, better consistancy in the energy density was obtained by pre-heating the rods of the laser.

Ultraviolet Reflectivity

The ultraviolet reflectivity measurements were made using the equipment and procedure which Mullins (Ref 8) had used in his work. As recommended by Mullins, the single Molectron Boxcar Integrator had been replaced by the two Princeton Applied Research (PAR) Boxcar Integrators. This was done in order to reduce the severe noise problems inherent in his particular equipment arrangement.

The method used for measuring the reflectivity, $R(\omega)$, over a wide spectral range was accomplished by simultaneously measuring both the incident and reflected intensities, I_o and I_r, respectively, then electronically dividing the signals. It was possible to use a single detector mode of operation to measure both I_o and I_r since the incident light beam was chopped. Thus, the use of a single detector eliminated the problem of ensuring both I_o and I_r be measured by detectors with identical spectral responses.

The mechanics of actually measuring I_o and I_r consisted of a spinning disk on which both the sample and a highly reflective mirror were mounted (Ref 20). As the disk spins, reflected light from the sample, I_r, and reference, I_o, mirrors alternately illuminate the detector. The detector yields an output signal which contains both I_o and I_r in an alternating fashion. The output signal is then resolved into its incident and

reflected components by the use of two boxcar integrators.

A boxcar integrator synchronously samples an input signal with variable width, variable delay gate, which can be fixed on any point on, or slowly scanned across the input signal. That signal passed by the gate is averaged by variable time constant integrators, the output of which is the average of some number of repetitions of the input signal over the gate width interval. Because the average value of noise over a large number of repetitions is zero, an improvement in signal-to-noise ratio occurs. If the gate is fixed on a single point of the input signal, the boxcar integrator output rises asymptotically toward the amplitude of the synchronous portion of the input signal at the sampled point. Thus, I_o and I_r are measured by individual boxcars since the boxcars are properly enabled in the timing sequence, Figure 6.

An aluminum mirror was used as the highly reflective surface within the spinning disk. Aluminum coatings, when properly applied, have a relatively flat reflectance spectrum over the wavelength range between 200 nm and 400 nm. Its reflectivity curve will vary by only 1% in this region, with a relatively high absolute reflectivity of approximately 92%. The method of deposition of aluminum on glass is discussed on Appendix A.

A modified version of the reflectometer designed by Beaglehole was used for all ultraviolet reflectivity measurements (Ref 20). Figure 7 details the experimental equipment. A Deuterium lamp was used to provide the incident light for

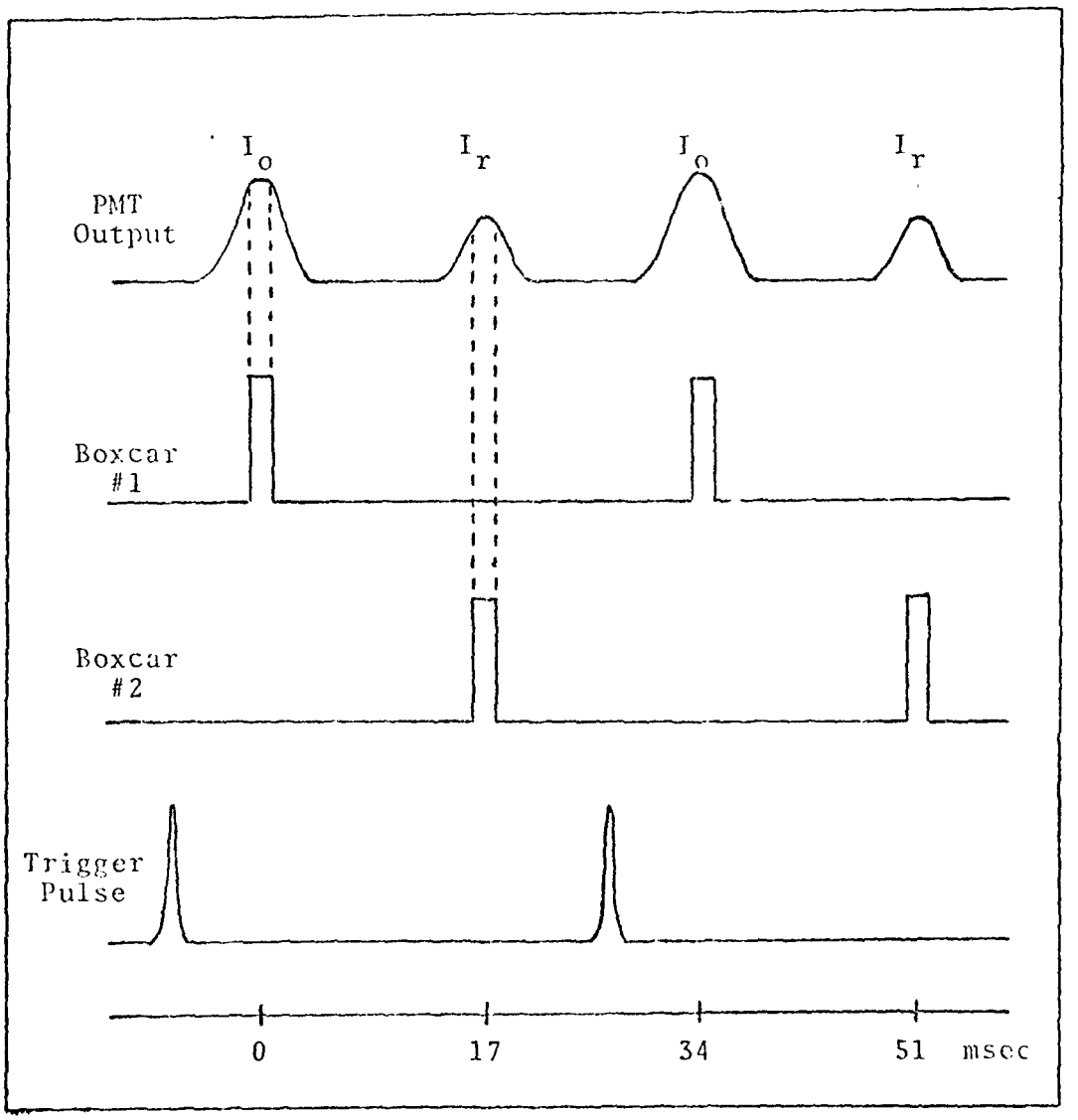

Fig 6. Boxcar Integrator Timing With Respect to Alternating PMT Output (Trigger provided by photo diode)

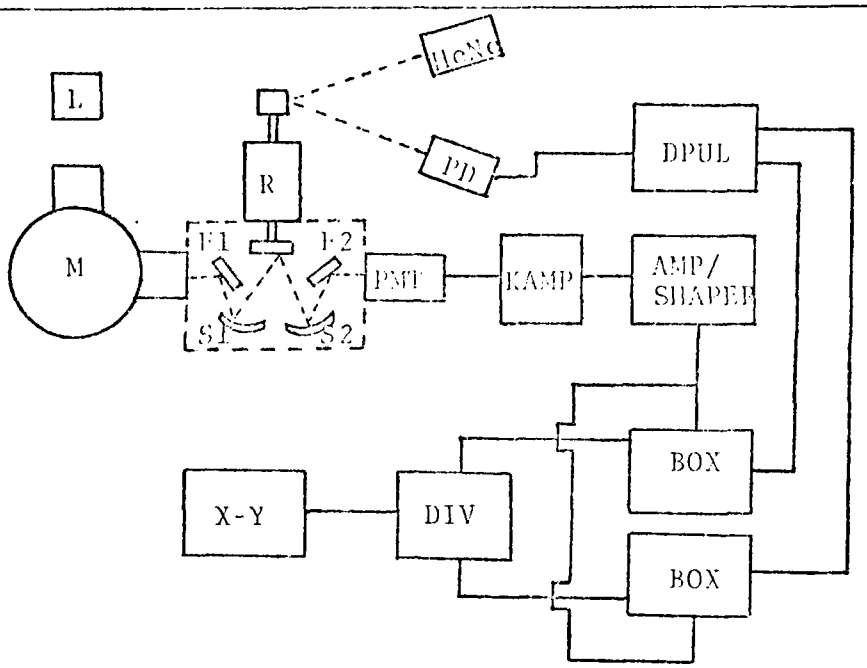

Symbol	Description
L	Oriel Model 6316 Deuterium Lamp Oriel Model 6310 Lamp Power Supply
M	Jarrel-Ash Model 78-650 One Meter Vacuum Scanning Monochromater
R	Rotary Device
S1,S2	Spherical Aluminum Coated Mirrors
F1,F2	Flat Aluminum Coated Mirrors
HeNe	Spectra Physics Inc., Model 142 HeNe Laser
PD	Photodiode 1N2175
PMT	RCA 4832 Photomultiplier Tube
KAMP	Keithley Model 427 Current Amplifier
AMP/SHAPER	Molectron Model 131 Amplifier/Shaper
BOX	Princeton Applied Research Model 160 Boxcar Integrators
DPUL	Hewlett-Packard Model 8010A Duel Pulse Generator
DIV	Molectron Model 151 Multiplier/Divider
X-Y	Hewlett-Packard Moseley Autograf Model 7001A X-Y Recorder

Fig 7. Optical Reflectivity Equipment

the monochromator entrance slit was never changed throughout the experiment. The monochromator was of the Seya-Namioka mount design, equipped with 650 micrometer slits and a Bausch and Lomb grating with 1200 grooves/mm and a blaze wavelength of 70 nm. The monochromator output was focused onto the spinning sample disk of the rotary device by use of mirrors F1 and S1. The rotary device is a trigger mirror and sample holder mounted on an AC synchronous motor (Fig. 8). The spinning sample holder contains the aluminum reference mirror and the sample. A cover plate with two apertures of .33 cm diameter is placed over the aluminum mirror and sample in order to provide for the chopped signal mode of operation. Mirrors S2 and F2 image the reflected beam from the sample disk onto the photo-multiplier tube. The output from the PMT was amplified and shaped using the Keithley and Molectron amplifiers. The output signal from the Molectron amplifier is then fed into both PAR boxcar integrators. The Hewlett-Packard dual pulse generator provides the enabling pulses to the integrators, thus separately measuring I_o and I_r. The integrated values for I_o and I_r were then divided by the use of the Molectron multiplier/divider unit and the ratio I_r/I_o was plotted on the X-Y recorder.

The dual pulse generator received its trigger pulse from a photodiode. The photodiode was used to detect a reflected HeNe light pulse reflected off a trigger mirror mounted on the spinning shaft of the rotor device. The dual pulse generator, via the trigger pulse from the photodiode, produced

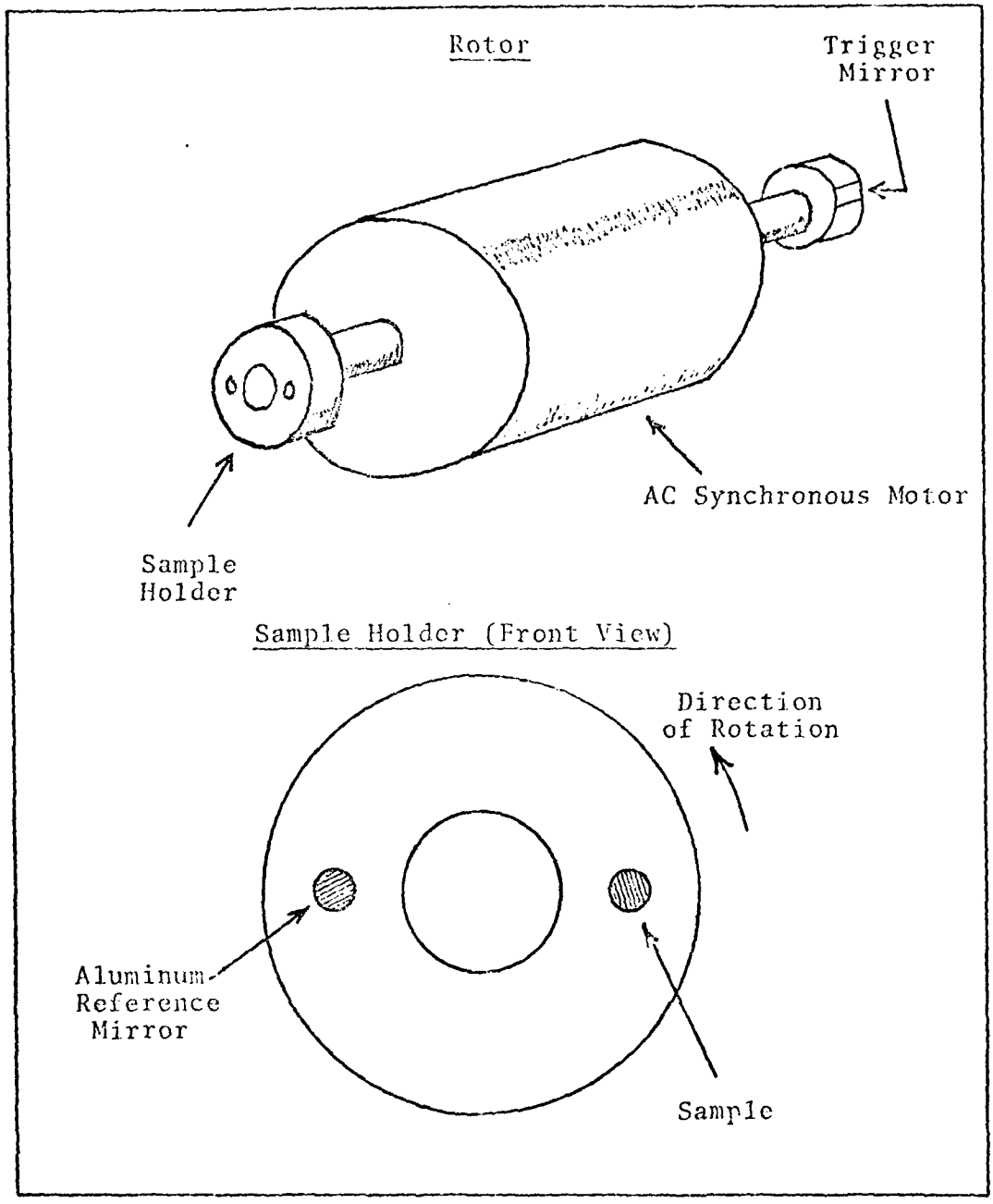

Fig 8. Rotary Device and Sample Holder

the properly delayed enabling pulses which synchronized the timing of the boxcar integrators with the rotor device. The timing between the PMT signal and the enabling pulses was monitored on a Tektronix Model 7904 oscilloscope.

The accuracy of measuring $R(\omega)$ and the absolute reflectivity was very good using this system. The changes in $R(\omega)$ of less than 1% were detected and an absolute value for $R(\omega)$ was accurate to $\pm.2\%$. These values were obtained by making several experimental runs with virgin, compensated, GaAs crystals. The spectra obtained was extremely consistent from run to run, and in fact, standard deviations of less than .1% was obtained for a single crystal for one complete data run. Hence, data runs for the sample were limited to one spectral scan since a high confidence in the equipment and procedure had been established.

UV Reflectivity Procedure

The GaAs sample and the aluminum reflective mirror were mounted within the sample holder of the rotor device. The plate mounted over the mirror and sample contained two .33 cm diameter apertures located 180° apart from each other. Care was taken to ensure that both the aluminum mirror and the sample were mounted on the same reference plane with respect to each other. This was accomplished by mounting the plate directly in contact with the mirror and sample. Thus, a small gap between the aperture plate and the sample holder could be compared at the 180° locations to ensure uniformity

(Fig. 9). The angle of incidence was approximately 8°, and the sample holder was rotated at 25 Hz. The PMT, at -1200V, had its dark current suppressed to zero using the noise suppression on the Keithley amplifier. The dark current, I_{ds}, must be suppressed or it adds to the signal current, I_{os} and I_{rs} of I_o and I_r, producing erroneous data since

$$R(\omega) = \frac{I_r}{I_o} = \frac{I_{rs}}{I_{os}} \neq \frac{I_{rs} + I_{ds}}{I_{os} + I_{ds}} \qquad (12)$$

The grating was fully illuminated by the Deuterium lamp placed at the entrance slit of the monochromator. With the sample holder spinning, the output from the PMT could be monitored with an oscilloscope. The enabling gates from the boxcar integrators could then be centered under the peak from each pulse, I_o and I_r, using the oscilloscope's duel trace capability (Fig. 6). A .15 msec enabling gate time was used for each integrator with a 34 msec time delay between gates.

Before each data run, the equipment was standardized to a common reference point. This was done in order to ensure that the limits of the multiplier/divider unit were never exceeded. The numerator, I_r, could range from 0 to +100 or 0 to -100 volts DC, while the denominator, I_o, could range from -1 to -10 volts, or +1 to +10 volts DC. The DC signal emanating from the boxcar measuring I_o (aluminum mirror) was always set for a maximum of -9.5 volts DC at the wavelength of 318 nm. The inputs to the multiplier/divider were inverted DC values, thus the output was also inverted. The input to the X-Y

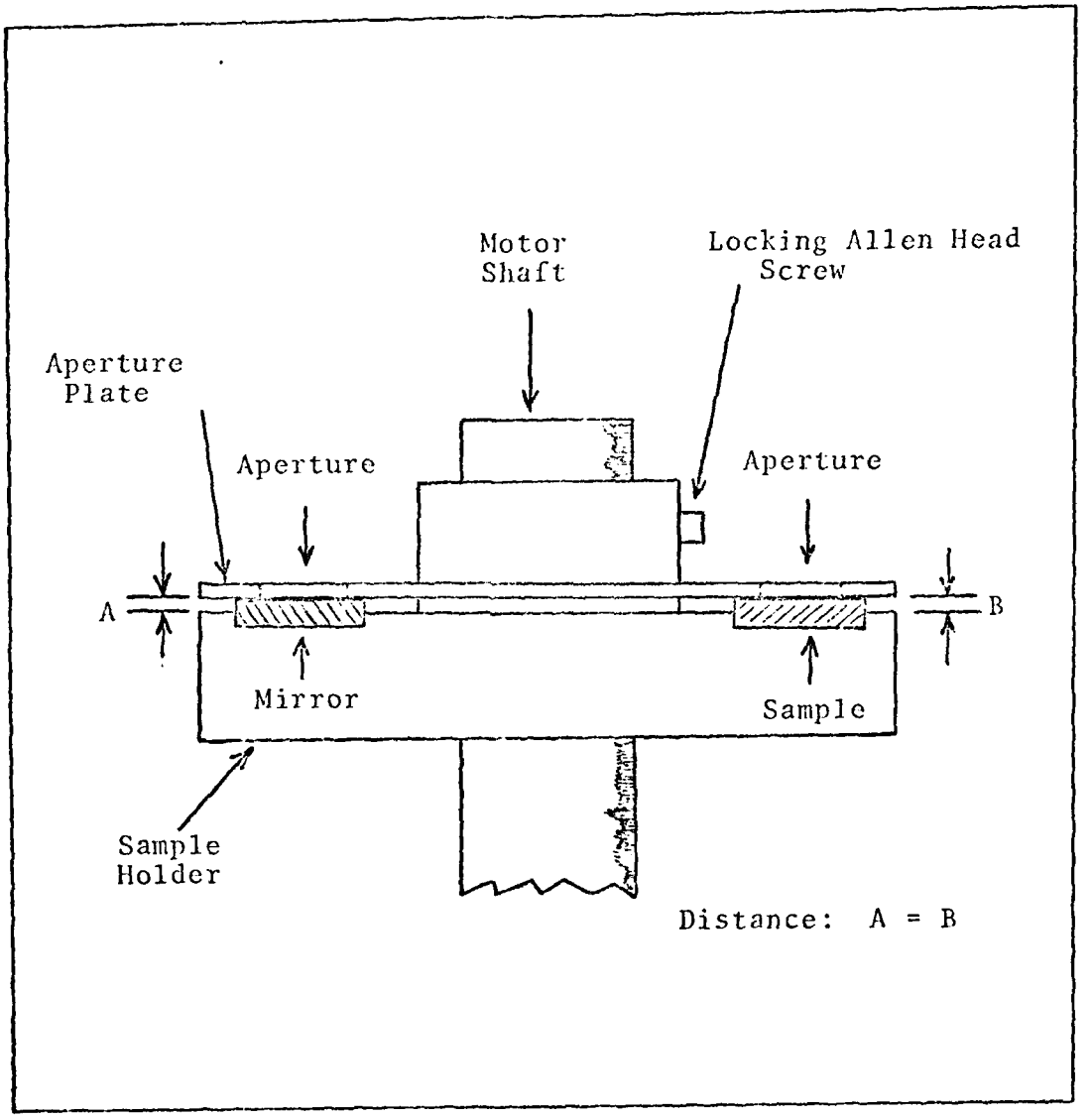

Fig 9. Side View of Sample Holder and Aperture Plate

recorder, being negative, was reversed biased in order to yield a positive reading on the spectral traces of the recorder.

To improve the resolution of the X-Y recorder of R, the zero and the variable volt/inch scale on the recorder was calibrated with respect to the I_o output of the multiplier/divider. Maximum scale settings were established at the 25% and 75% value for I_o. Thus, full scale deflection on the recorder ranged from 25% to 75%, yielding resolution for the absolute R in the range of .1%. As each spectral scan was made, absolute reflectivities for the sample surface (where $R = I_r/I_o$) at any wavelength between 210 nm to 380 nm was directly recorded and available as data.

The scanning rate of the monochromater was 150Å/minute. Every 100Å, a tick mark was placed on the graph paper of the recorder in order to locate specific wavelengths for the peak and valley of the reflectance profile of the sample. After $R(\omega)$ was plotted, the values for D, the degree of damage, were then calculated from the values of R at the peak and valley wavelengths of 247 nm and 335 nm, respectively.

Each sample was prepared in a similar manner just prior to a UV reflectance data run. Each sample was rinsed in isopropyl alcohol, then dried using optical tissue. If the sample was one which was being etched, then after the chemical etch, the sample was rinsed in distilled water, then rinsed in isopropyl alcohol, with a drying by use of the optical tissue.

General Experimental Procedure

All the GaAs samples used, whether virgin or as-implanted, were from the same boule. However, it was doubtful that the same samples came from the same wafer since many more samples were used than are normally cut from a single wafer, and later evidence of surface reflectivities seemed to group the samples into particular sets (see Chapter IV). The virgin GaAs crystals were grown by the Bridgeman method, were chromium compensated, and in a <100> orientation. The ion implanted samples were 120 keV selenium at 10^{14} ions/cm^2. The depth of penetration of the selenium ions, according to LSS theory (Ref 1), had a projected range of 400Å ± 200Å depth from the surface of the substrate.

The approach used in attempting to determine whether the damage coefficient, D, improved under some optimum laser multipulse sequence consisted of annealing of the sample, then performing UV reflectivity measurements on the surface or on the various etched surface layers. From this, a damage coefficient, D, was obtained for each surface layer, with ultimately a D versus depth profile relationship. This profile was compared with the as-implanted depth profile of GaAs. If improvement was detected by the way the D versus depth profile improved, then it was assumed the multipulse sequence was close to an optimum level for successful laser annealing.

Specifically, first an $R(\omega)$ spectral profile for the

surface of the virgin GaAs was obtained. This was done in order to establish a reference spectral profile to which all subsequent $R(\omega)$'s of implanted samples, whether annealed or unannealed, could be compared to. Also, this profile provided the data required for the crystalline terms of the equation used in the calculation of D, the damage coefficient (Eq 11). The virgin sample was then etched in layers of 100Å to a depth of 1000Å, in order to yield information of the variance of $R(\omega)$ with respect to depth. This 1000Å depth of etch was well through the expected maximum damage depth of the implanted crystal since the LSS projected range of concentration was to a depth of 400Å ± 200Å. All etching was performed using a solution of 50:1:1 of distilled water, H_2SO_4 and H_2O_2. This etching solution, maintained in an ice bath, was under constant agitation by use of a magnetic stirrer. Each day of etching was begun with the mixing of a fresh etching solution.

After completing the profiling of the virgin sample, the procedure was repeated using an unannealed implanted sample. The same etching technique was used as in the virgin samples. A D versus depth profile was obtained, thus establishing the reference profile to which all annealed samples would be compared to.

With the profiling complete for both the virgin and unannealed Se implanted GaAs, the next step was to actually laser irradiate the substrates with single bursts of 15 nsec pulses of .53μ wavelength irradiation. The first samples irradiated were the virgin GaAs in order to determine maximum

and minimum surface effects with respect to the .53μ wavelength energy density levels used. The surface reflectivity for each sample irradiated at a different energy density level was obtained, thus yielding a relationship of D versus E_d.

The next phase required the above procedure to be repeated for implanted samples. Once again, surface reflectivities for each sample was obtained, thus yielding a relationship of D versus E_d. From this D versus E_d relationship, an E_d level was picked, thus establishing an optimum multipulsing E_d range. This E_d level was based on the criteria of: the E_d point on the curve of D versus E_d, which yields the minimum D level, is the optimum E_d level for this .53μ wavelength, Q-switched, laser being used in the experiment.

The final process of the experiment involved the actual multipulsing of the implanted samples. The samples each were multipulsed once, twice, four, eight, and twelve times, respectively. Each sample was then analyzed for the D versus depth profile in order to determine the extent of repair at the various multipulse numbers.

IV. Results and Conclusions

Results

The use of D, the damage coefficient, as a means of determining the crystallinity of GaAs surfaces can only be considered a rough first order measurement. Fundamental differences in the dose dependence of the optical reflectivity spectra exist between silicon and GaAs which limits the applicability of D in the case of GaAs.

The D coefficient (see page 16) is determined using the absolute reflectivity of a sample at the wavelengths which are the peak and valley points of the $R(\omega)$. In the case of the GaAs, the R_1 and R_2 points were at 2470Å and 3350Å, respectively. The validity of D is based on the premise that the absolute reflectivity at the R_2 valley point will remain constant for a change in a material's crystalline to amorphous state (Ref 9). If this condition is fulfilled, then the relative reflectivity at the R_1 peak point can be measured with reference to reflectivity at R_2. This yields a parameter whose change is proportional to the degree of damage, namely D.

In the case of silicon, Miyao, et al. (Ref 9) did confirm results reported by Yen, et al. (Ref 27) that the R_2 valley point at 3300Å did not vary by more than 1-3% for various ion implant doses. Miyao was able to show that the

D coefficient was in good agreement with damage values obtained using Rutherford backscattering and electron spin resonance measurements. This suggests two points in the case of silicon: . 1) the R_1 peak point changed in proportion to the degree of damage on the silicon, and 2) the R_2 valley point did not change in reflectivity with changes in the degree of damage.

Similar studies with GaAs show a change in the absolute reflectivities at the R_1 peak and R_2 valley points with respect to the material's degree of damage due to ion implants. For instance, Shifrin, et al. (Ref 23), using Cd* implanted GaAs in the dose range of 10^{12} to $8x10^{14}$ ions/cm^2, found that the R_1 peak changed from 64% for the crystalline material to 53% for a dose of $1.5x10^{13}$/cm^2. The change in the R_2 valley point for the crystalline material was from 43% to 39% at the dose of $1.5x10^{13}$/cm^2. At the dose of $8x10^{14}$/cm^2, the R_1 peak further decreased to 35%, whereas the R_2 valley point increased to 41%. Thus, the total range of change in the reflectivity of R_2 was 4.5%. The total range of change for the R_1 peak was 29%. Also, Grasso, et al. (Ref 24), reported Te implanted GaAs at a dose of 10^{15}/cm^2 caused the absolute reflectivity of the R_1 peak point to decrease from 59% for the crystalline material to 44% for the implanted material. The R_2 valley point actually increased from 37% for crystalline material to 43% for the implanted material. Thus, the total change for the R_1 peak point was 15%, and the R_2 valley point was increased by 6%.

The results of the experiments of the preceding paragraph indicate a greater dependence on lattice damage in the R_2 valley reflectivity (with respect to dose) in the case of GaAs when compared to the silicon results obtained by Miyao, et al. (Ref 9). Miyao had estimated the dependence in the silicon reflectivity at the R_2 valley to be about 1-3%. This dependence, as reported by Miyao, yields not more than a 10% fluctuation in the calculated value of D. Similarly, in the case of GaAs, the greater dependence of the reflectivity at the R_2 valley point yields a fluctuation in D which can be as much as 20%.

The $R(\omega)$ for the surface of unannealed virgin GaAs is shown in Fig 10. The spectral response is the average of two separate samples from the same boule. The standard deviation was not greater than 1.45% for the two samples. The surfaces were cleaned prior to the reflectivity measurements using the procedure described in Chapter III. The peak of R_1 was measured at 247 nm, and the R_2 valley point at 335 nm.

The virgin samples were then etched in order to determine the variance of R_1 and R_2 with respect to depth and possible effects due to preferential etching. Table I, showing the results of the etching of the two samples, indicates a generally decreasing R_1 value at etching progressed to deeper layers. Also, the difference between R_1 and R_2, the peak and valley, was found to decrease. This R_1-R_2 term is is pivotal in the calculation of D (see Eq 11). Hence, the calculation for D was made with respect to the actual R_1 and

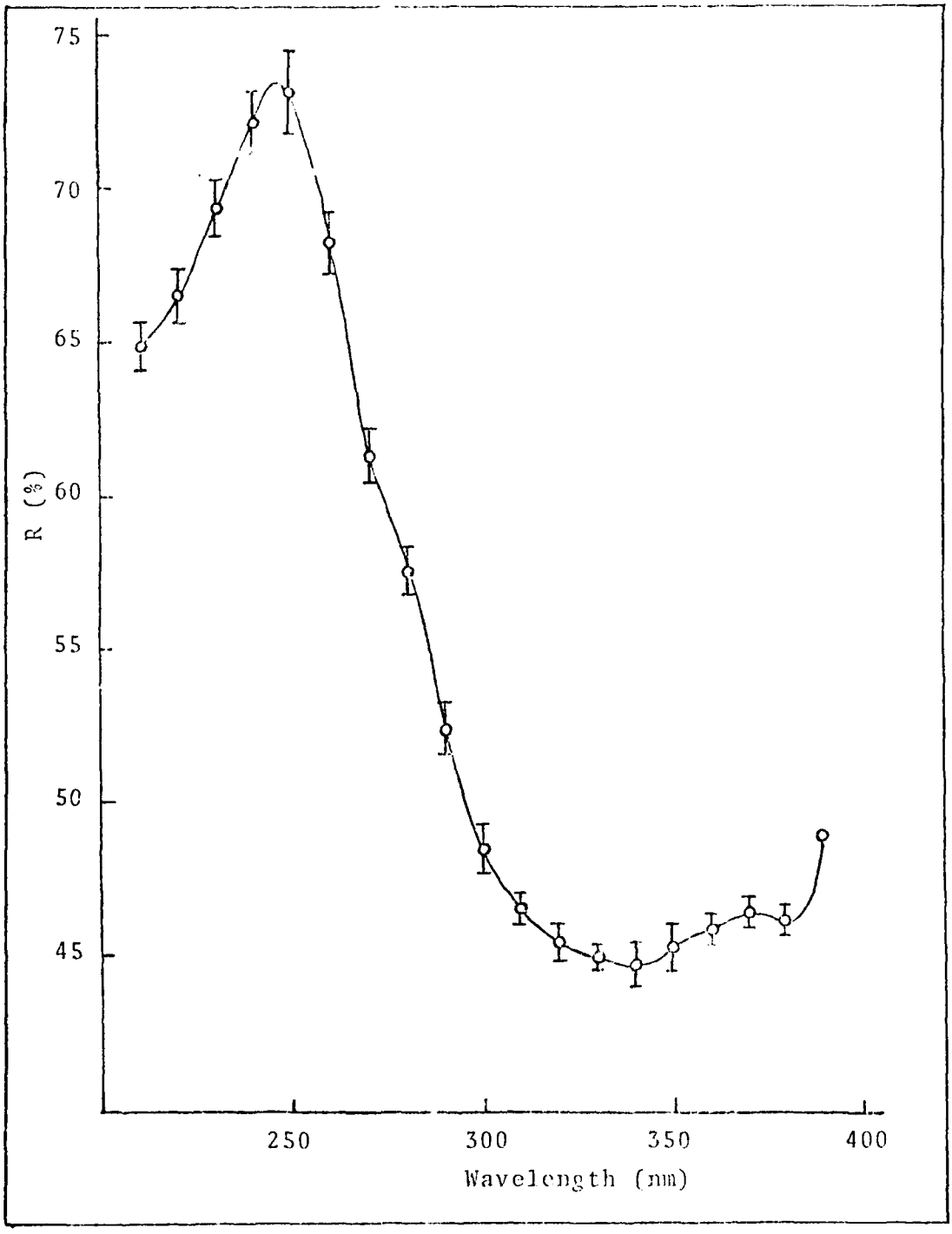

Fig 10. Surface Reflectivity Spectra of Unannealed Virgin GaAs

TABLE I

Variance of R(%) With Respect to

Depth for Two Virgin GaAs Samples

Depth, Å	Sample #1			Sample #2		
	R_1	R_2	R_1-R_2	R_1	R_2	R_1-R_2
Surface	72.2	44.2	28	74.3	45.2	29.1
100	71.3	45.6	25.7	70.5	44.3	26.2
200	71.3	46.8	24.5	69.9	44.3	25.6
300	68.3	44.5	23.8	67.1	42.1	25
400	66.8	42	24.8	65.2	41.1	24.1
500	61.3	39	22.3	69.7	44.9	24.8
600	65.9	43.1	22.8	64.8	41	23.8
700	68.3	45.4	22.9	66.5	42.7	23.8
800	59.8	39.8	20.6	64.2	40.7	23.5
1000	65.2	43.4	21.8	61.8	40.7	21.1

R_2 value at each respective layer.

The graph of Fig 11 shows the $R(\omega)$ for etched layers of the Se implanted GaAs. On the surface of the implanted sample, there is a smoothing out of the R_1 peak along with a general downward slope of this particular spectra. As the etching proceeds to the 100Å and 200Å depths, the slope flattens with still no R_1 peak apparently visible. At 400Å, the R_1 peak begins to dominate the spectra. The R_2 valley has changed from 53% at the surface to 42% at the depth of 400Å. The lattice disorder caused by the implantation is transitioning from a maximum disorder at 200Å to a lesser degree of disorder at 400Å. At 600Å depth, the R_1 peak has emerged, reaching a reflectivity level approaching that of virgin GaAs. At the 600Å depth, the R_1 peak is 63%, compared to virgin crystalline material which is 73%. The R_2 valley is 42%, compared to crystalline material which is 44%. The transition of the reflectivities from that of virgin crystalline materials to that of implanted materials compares with similar results obtained by Grasso, et al. (Ref 24). He states that in the R_2 valley point there is first a slight increase in the reflectivity before decreasing with greater dose. This can be seen in Fig 11 where on the surface the R_2 valley at 3350Å first increases from 44% to 53%. As the depth is increased, the concentration also increases and the R_2 reflectivity then decreases. As the concentration eventually begins to decrease, the R_2 reflectivity begins to increase back toward 44%.

The damage profile curve of Fig 12 is derived from the

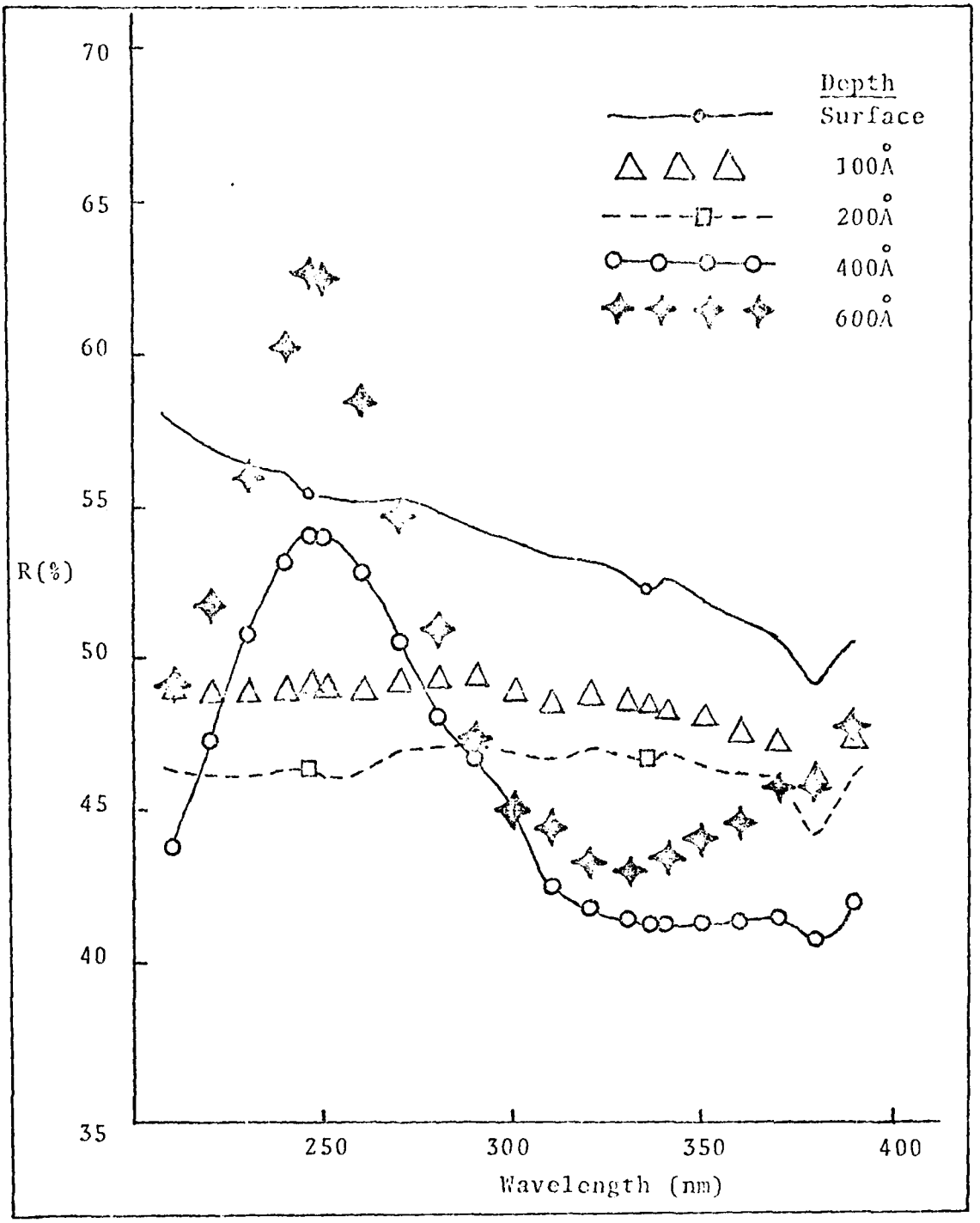

Fig 11. $R(\omega)$ for Etched Layers of Se Implanted GaAs, 120 keV; Fluence is 10^{14} ions/cm^2

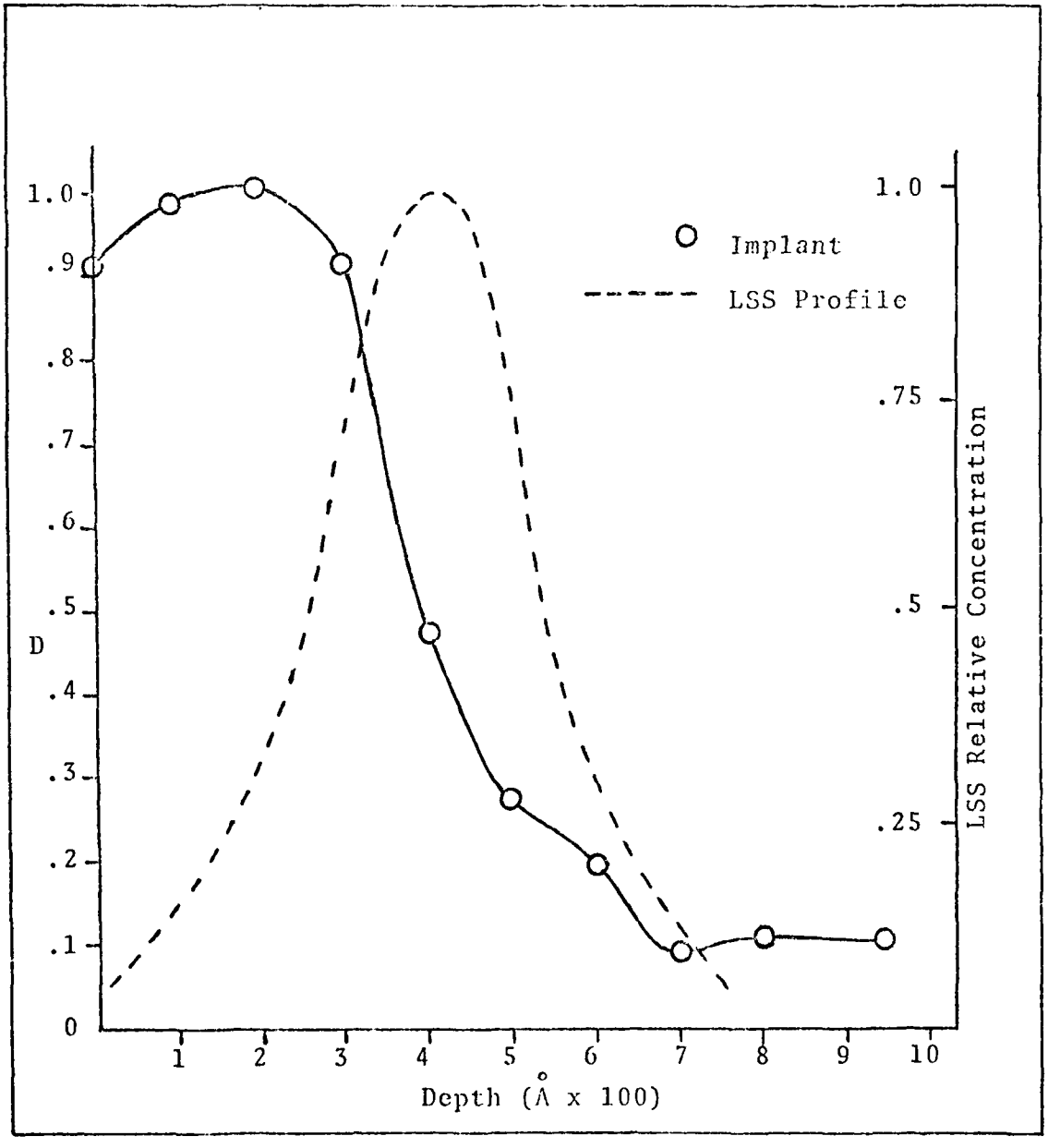

Fig 12. Damage Versus Depth and LSS Profile for Unannealed Se Implanted GaAs

data on Fig 11. This result is similar to that of Kim, et al. (Ref 25), who used Mg implanted GaAs, $10^{15}/cm^2$. He was able to show good correlation with damage profile theory. Similarly, the damage profile of Fig 12 agrees very nicely with damage profile theory for ion implants (Ref 26). The fact that Fig 12 agrees with theory enforces the validity of the curves of Fig 11. Thus, in Fig 11, the $R(\omega)$ obtained at each layer for the implanted sample is a good representation of the actual changes in R_1 and R_2 with respect to depth and various concentrations of implant dose.

The implant profile of Fig 12 establishes the reference which is to be improved by multipulsing. The optimum energy density, E_d, at which to anneal was determined by single pulsing four virgin and five implanted samples. The E_d level ranged from .12 to .446 J/cm^2 for the virgin samples and .048 to .442 J/cm^2 for the implanted samples. The results for the surface $R(\omega)$ after single pulsing are shown in Figs 13 through 16. From the data of Figs 13 through 16, a damage coefficient D versus E_d is developed. Figure 17 shows this result. The E_d level which appears to be optimum for multipulsing is .290-.300 J/cm^2, since at this level the D coefficient is a minimum.

Each of the samples were inspected for visible surface damage using a medium power microscope. At the range of .29-.3 J/cm^2, no surface effects could be seen with either the virgin or implanted samples. However, both the virgin and implanted sample which had been irradiated at the .42 and

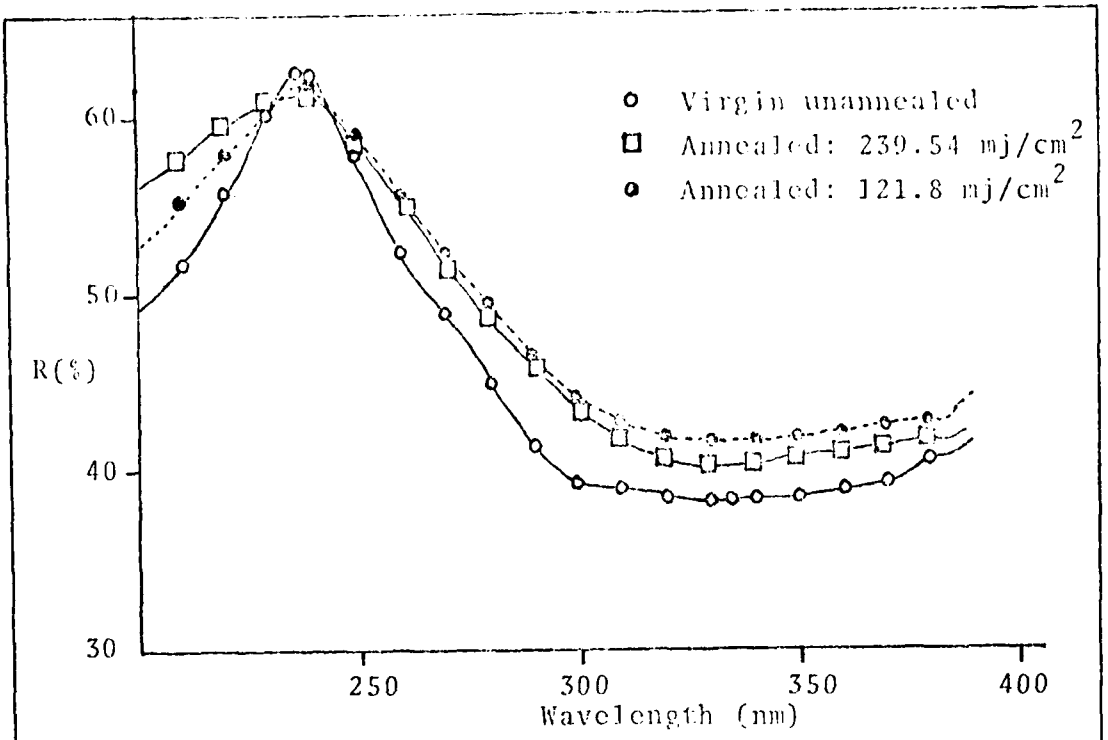

Fig 13. Surface R(ω) for Single Pulsed Annealed Virgin GaAs at Various E_d

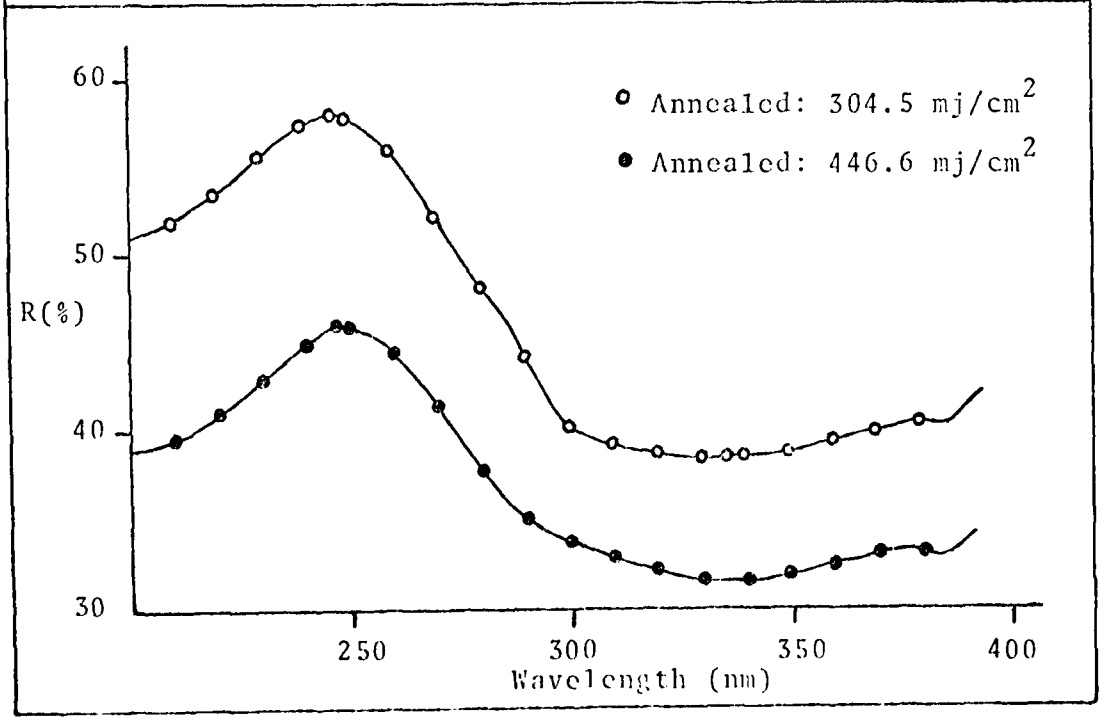

Fig 14. Surface R(ω) for Single Pulsed Annealed Virgin GaAs at Various E_d

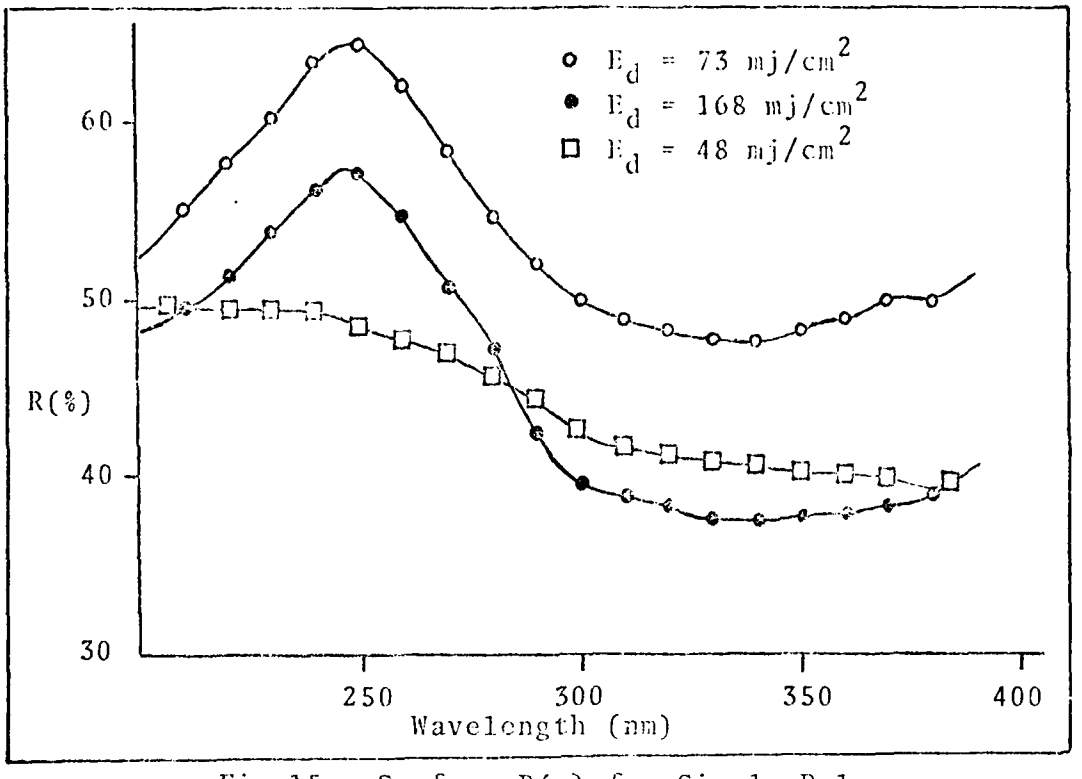

Fig 15. Surface R(ω) for Single Pulse Annealed Se Implanted GaAs at Various E_d

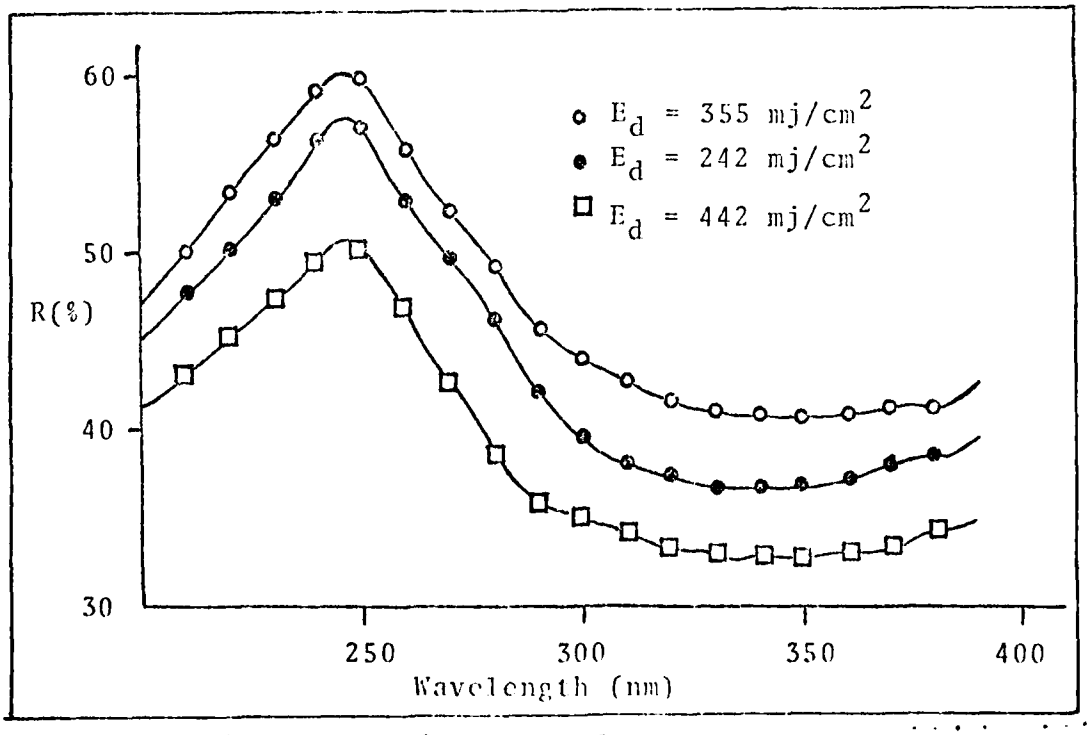

Fig 16. Surface R(ω) for Single Pulse Annealed Se Implanted GaAs at Various E_d

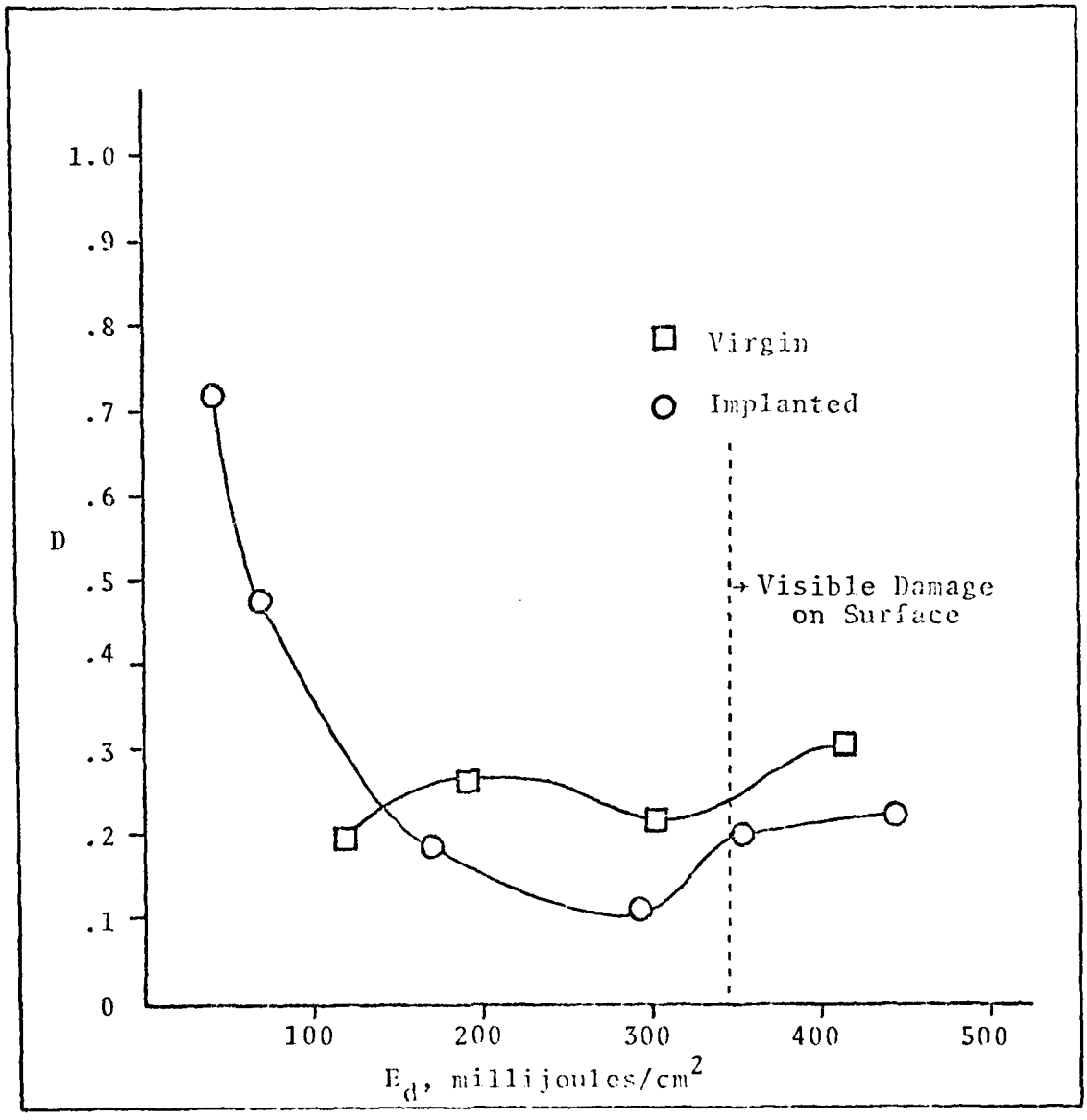

Fig 17. Damage Coefficient, D, Versus Energy Density, E_d, for Single Pulsed Laser Annealed GaAs

.44 J/cm^2 E_d level exhibited large areas of cratering and clusters of bubble-like spots. At levels below .29 J/cm^2, no effect upon the surface could be seen at all.

The virgin samples plotted on Fig 17 have a damage coefficient which is higher than that of the implanted material. However, the virgin material shows a minimum D at an E_d of 300 mj/cm^2 which is comparable to that of the implanted samples with a minimum D at 290 mj/cm^2. The significance of the fact that the virgin samples did not re-form back to a crystalline state whose damage coefficient was equal to zero is not known at this time. It can be speculated, as in the case of thermal annealing, that there is a decomposition of the crystal (perhaps through the loss of arsenic) (Ref 25), which is effecting the crystal lattice order. However, as the E_d is increased, the arsenic loss also increases. This is shown by the increase of D at the higher E_d of 400 mj/cm^2.

The multipulsing was performed using six implanted samples. Each of the six samples were pulsed, first with a single pulse at the target E_d of .29 to .3 J/cm^2. A slight fluctuation of actual E_d existed from pulse to pulse. Consequently, the range of E_d for the first set of pulses was varied. As can be seen in Table II for samples numbered 1, 2, and 3, the E_d was about 12% higher than intended.

The R(ω) at etched layers of 100Å was examined to a depth of 1000A for samples #1 and #2. From the R(ω), the D coefficient was obtained in the usual manner. This result is shown in Fig 18. The etched profile for an unannealed

TABLE II

Pulse Energy Density for

Multipulsed Annealed Samples

Total Pulses	Energy Density (J/cm^2)					
	Sample					
	1	2	3	4	5	6
1	.357	.332	.333	.289	.300	.276
2	---	---	.312	.284	.274	.284
4	---	---	---	.284	.292	.300
	---	---	---	.300	.304	.304
8	---	---	---	---	.292	.300
	---	---	---	---	.292	.268
	---	---	---	---	.300	.300
	---	---	---	---	.308	.284
12	---	---	---	---	---	.292
	---	---	---	---	---	.300
	---	---	---	---	---	.292
	---	---	---	---	---	.284

implanted sample (from Fig 12) is included in order to compare crystallinity improvement. A decrease in the damage crystal profile is readily apparent. At the 200Å level, the D coefficient has decreased from 1.0 down to .25, which indicates a crystalline repair process has occurred.

The samples numbered 3, 4, 5, and 6 were then pulsed a second time. The E_d levels are shown in Table II. Sample #3 was then etched to determine the D coefficient versus depth profile. Figure 19 shows the results of sample #3's profile compared to that of an unannealed implanted sample. The crystalline repair process is more extensive as compared to that of the single pulsed samples. In fact, in the 100Å through 300Å depth, the D coefficient is zero, which would indicate crystalline material has been formed.

The remaining samples were multipulsed several times. The number of pulses and the E_d level for each pulse is listed on Table II. Sample #4 was pulsed a total of four times, sample #5 a total of eight times, and the last sample twelve times. Each sample was then etched and profiled in the same manner as that of the previous samples.

The etching profile for samples #4, #5, and #6 is seen on Fig 20. The unannealed implanted profile is also included for comparison. The three profiles exhibit the same general pattern with no particular trend towards improvement of the D coefficient at the peak located at the depth of 400Å. It can be assumed that a further increase in pulses would continue to yield a similar D profile since the twelve-pulsed

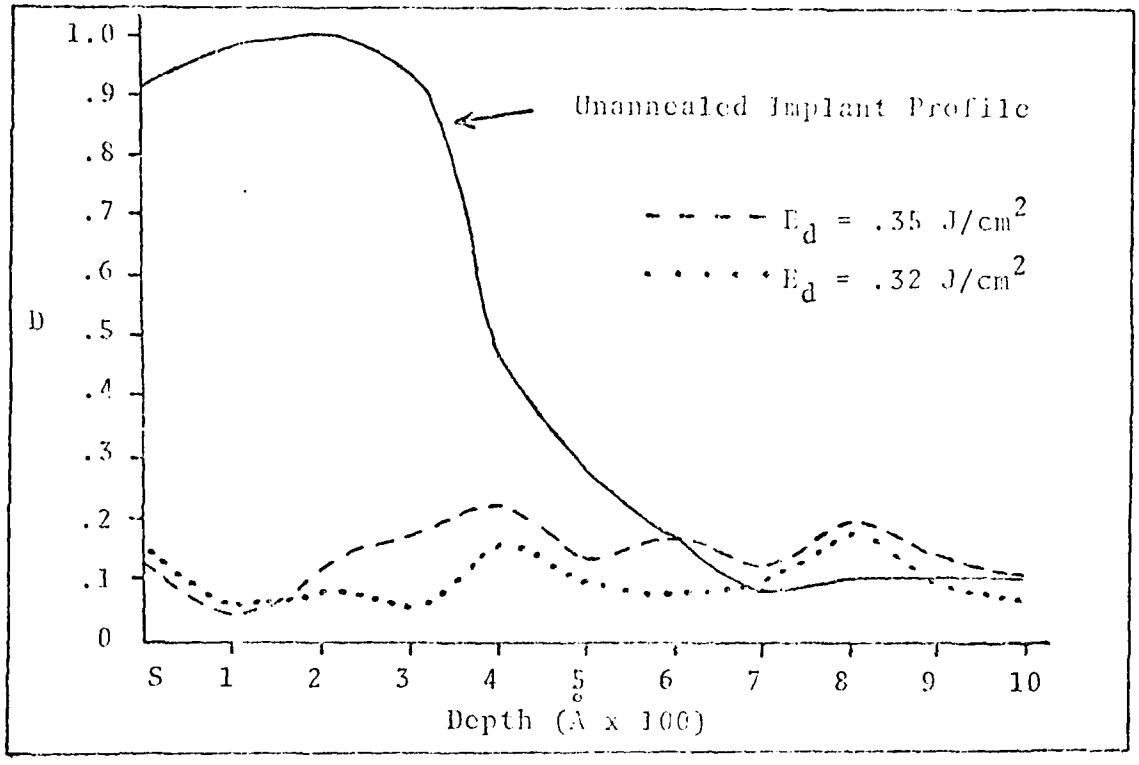

Fig 18. Damage Versus Depth Profile for Single Pulsed Annealed Implanted GaAs

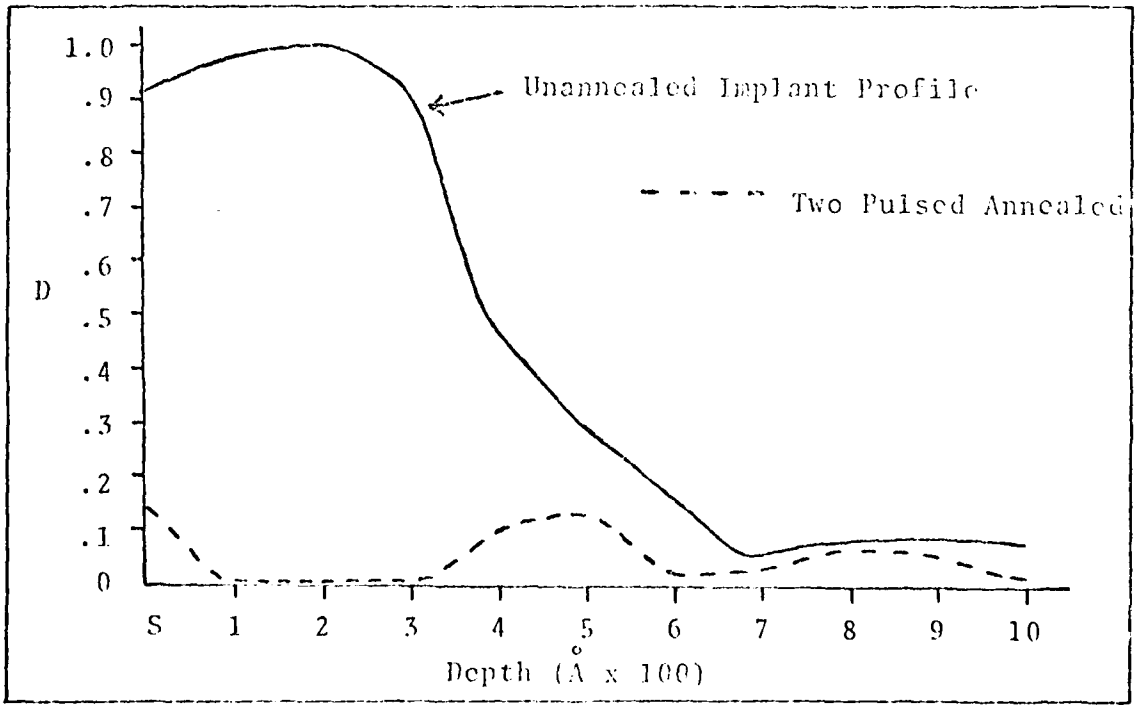

Fig 19. Damage Versus Depth Profile for Two Pulsed Annealed Implanted GaAs

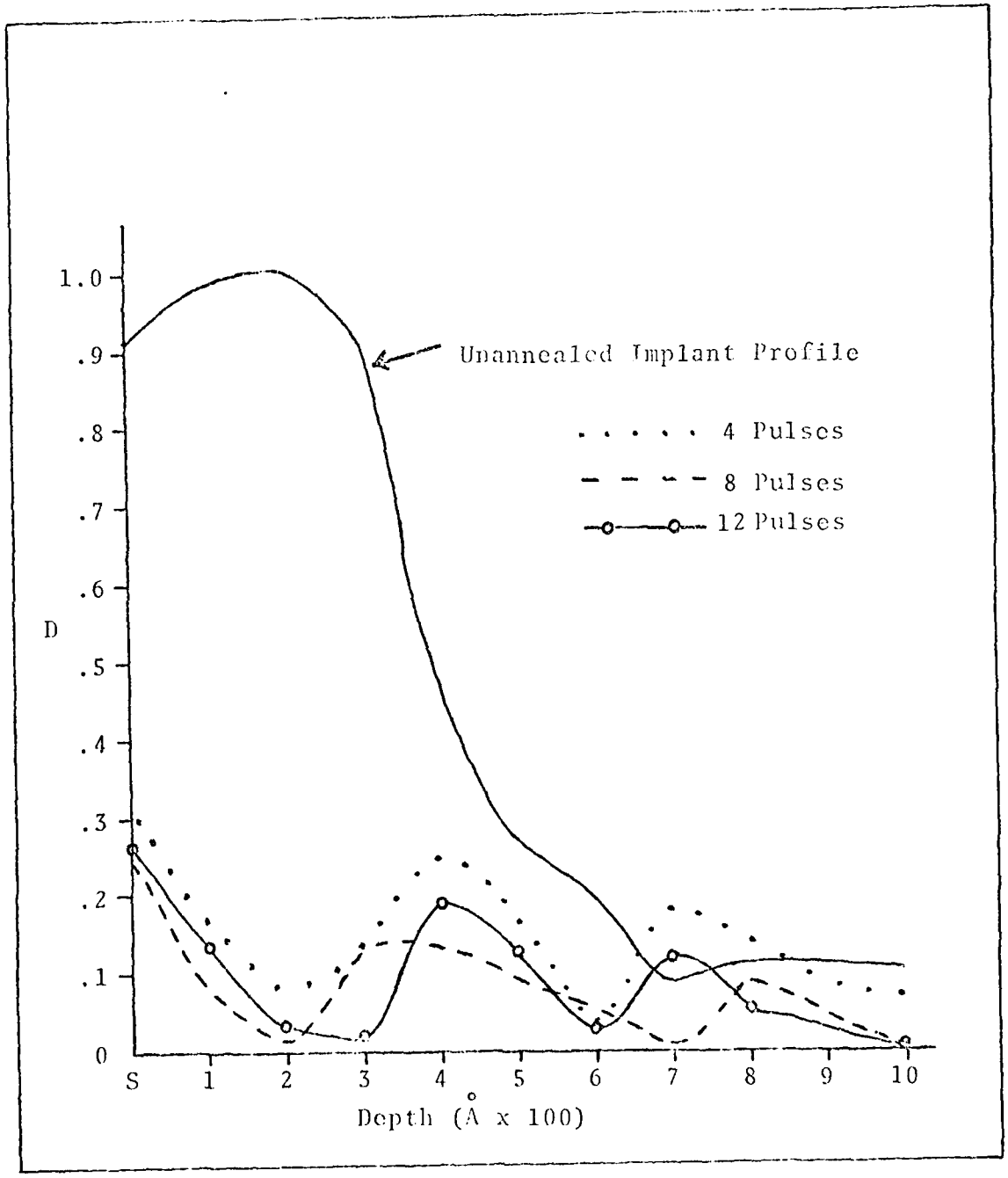

Fig 20. D Versus Depth Profile for Multipulsed Annealed Implanted GaAs

sample did not show a marked improvement over the four-pulsed sample.

A consolidation of all the damage profiles for the various pulsed numbers can be seen in Fig 21. Examination of the profiles reveals that the two-pulsed sample yields the best indication of damaged crystalline repair. The two-pulsed sample shows a D = 0 region existing between the depths of 100Å to 300Å. The indication within this region is that all damaged crystalline layers were repaired as a result of the two-pulsed laser anneal. In the two-pulsed sample, there are also peak damage location (D ≥ .12) at the surface and at depths of 500Å and 800Å. The peaks fit a general cyclical pattern which is similar for all of the multipulsed samples.

The source of the cyclical pattern of Fig 21 was investigated. The purpose of the investigation was to determine which term in the D calculation (Eq 11) is responsible for the pattern. Using the data from the two-pulsed sample, each term in the equation, R_1 and R_2, for both the crystalline and annealed samples, were plotted with respect to depth and compared to the D versus depth curve for the two-pulsed sample (Fig 19). The crystalline and sample terms plotted were: R_1, R_2, R_1-R_2, $1/R_2$, and $(R_1-R_2)/R_2$. It was found that the source of the pattern was the $1/R_2$ term for the crystalline material. This was based on the fact that the crystalline $1/R_2$ term yielded a curve whose cyclical pattern was very similar to the cyclical pattern of Fig 19. Also, the similarities in the curves of Fig 21 can be explained by the fact that

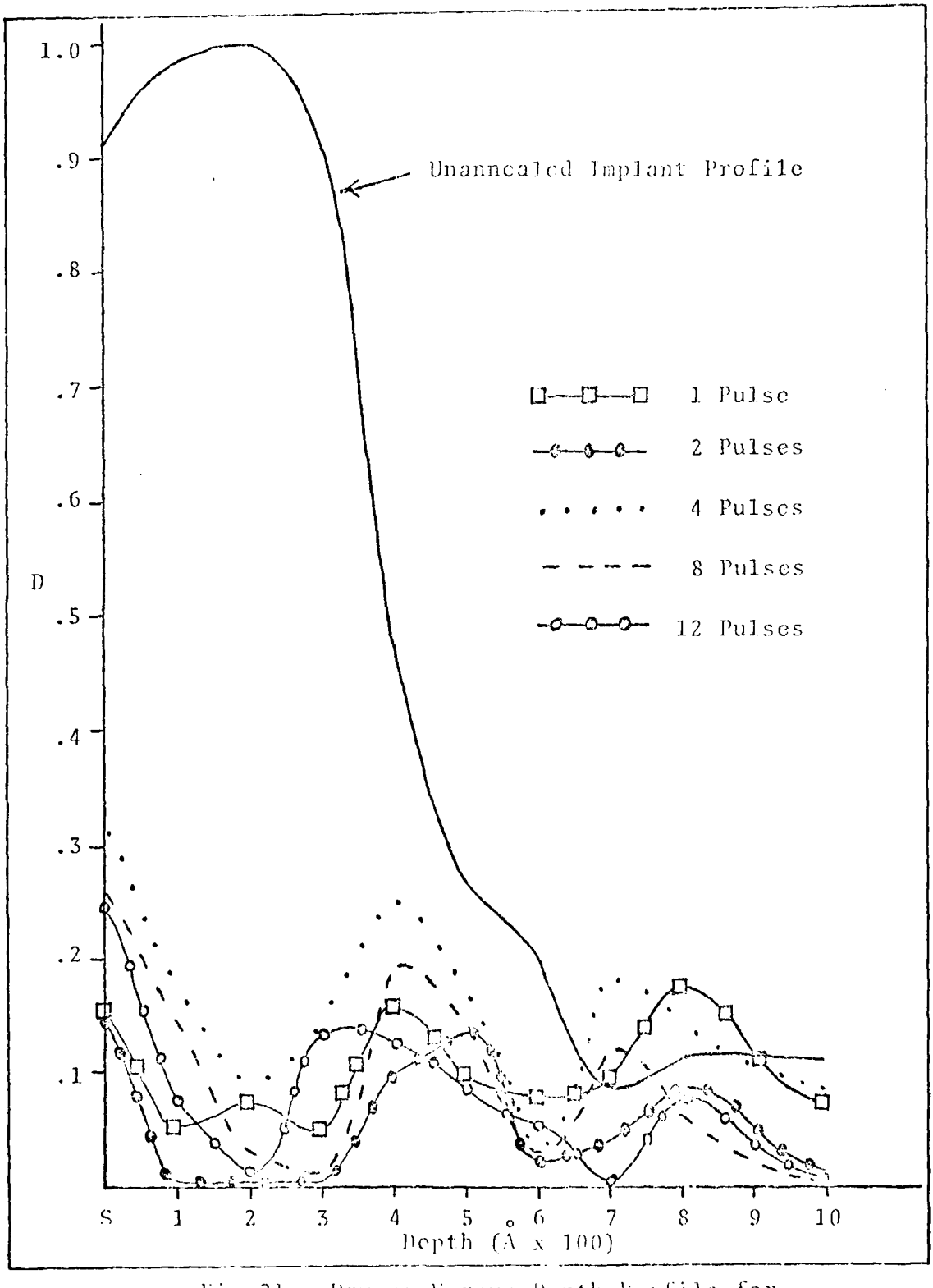

Fig 21. Damage Versus Depth Profile for Multipulsed Annealed Implanted Samples

this same $1/R_2$ term is used in the D calculation for each multipulsed sample.

The exact nature of the fluctuations of the crystalline material's reflectivity at the R_2 valley point with respect to depth is not known. Some possible sources of the fluctuations of R_2 could be in: 1) the electronics devices of the optical reflectivity equipment, 2) variations in the aluminum reference mirror, 3) effects of preferential etching, or 4) a real indication of variations of the absolute reflectivity at the R_2 valley point at various etched layers. Further investigation will be required to pinpoint the exact source of the cyclical nature.

Conclusions

The validity of D, the damage coefficient, was found to be a rough first order measurement of the degree of damage of crystalline surfaces in GaAs. This stems from the fact that GaAs when compared to silicon possesses fundamental differences in the dose dependence of the optical reflectivity which limits the applicability of D in the case of GaAs. However, useful contrasting damage profiles were obtained between as-implanted and annealed samples which were used to determine the applicability of laser annealing using the frequency doubled Neodymium:YAG laser and a multipulse technique.

The selenium implanted GaAs samples annealed at multipulse numbers of 1, 2, 4, 8, and 12 pulses all yielded a

dramatic reduction in the damage coefficient when compared to the D versus depth profile of an as-implanted sample (Fig 21). The two-pulsed laser anneal had the highest degree of recrystallization which approached that of virgin materials.

The optimum laser energy density for this experiment using the .53μ laser irradiation and a FWHM pulse of 15 nsec, was found to be within the range of 290 to 300 mj/cm^2 (Fig 17). The type of crystalline regrowth was most probably liquid phase epitaxial since the pulse width of the laser was very short. It is not known whether the crystal regrowth consisted of single crystal, poly-crystal, or a combination of both throughout the post-annealed implanted layers.

A cyclical pattern which was similar to all of the annealed samples (Fig 21) was due to the reflectivity, R_2, measured at 3350Å for the crystalline sample. The nature of the variance of R_2 with respect to depth requires further investigation.

The primary goal of this paper was accomplished since it can be shown that Se implanted GaAs can be annealed with a multipulse technique of two pulses using .53μ laser energy with an energy density of .3 J/cm^2. The R(ω) measurements of the substrate indicated that the crystallinity after two pulses approached that of a virgin substrate of GaAs.

V. Recommendation

Multipulse laser annealing of Se implanted GaAs using the .53μ pulsed laser energy has proven to be quite promising. The damage profile of the as-implanted samples was improved dramatically at the multipulse range of two pulses. However, the cyclical pattern which emerged for each multipulse number (Fig. 21) is disturbing since it is not known whether this is due to reflectivity procedures/equipment, chemical etching procedures, or indeed, is a true indication of $R(\omega)$ of the crystal. Information in this regard could be obtained by repeating this procedure of multipulsing using samples from other melts implanted to the same fluence and implant energy. A study of the correlation aspects between the repeated procedure and the original data may resolve the origin of the cyclical pattern.

The question of whether the dopant has been annealed into the crystal substitutionally can only be answered by extensive electrical activation testing. It is recommended the samples which are annealed at various multipulse numbers, each be tested for the electrical parameters of sheet conductivity, mobility, test activation, and type conductivity. Also, these parameters should be obtained as a function of depth. This data could then be used to compare the merits of this laser annealing procedure with that of thermal annealing.

Bibliography

1. Gibbons, J.F. "Ion Implantation in Semiconductors--Part I, Range Distribution Theory and Experiments," Proceedings of the IEEE, 56(3):295-318 (March 1968).

2. _____. "Ion Implantation in Semiconductors--Part II, Damage Production and Annealing," Proceedings of the IEEE, 60:1062 (1972).

3. "Search and Discovery: Laser Annealing Shows Promise for Making P-N Junctions," Physics Today, July 1978.

4. Bloemberger, N. "Fundamentals of Laser-Solid Interactions," American Institute of Physics Conference Proceedings, 50: 1-9 (1978).

5. Fan, J.C.C., et al. "Annealing of Se-Implanted GaAs and InP by Scanned Nd: YAG Laser Irradiation," 7th Inter-National Symposium on GaAs & Related Compounds, St. Louis, Missouri, 27 September 1978.

6. Mason, Robert S. "Laser Annealing of Ion Implanted Gallium Arsenide." M.S. thesis. Wright-Patterson AFB, Ohio: Air Force Institute of Technology, December 1978. (AFIT/GEO/PH/78D-3).

7. Golovchenko, J.A., and T.N.C. Venkatesan, "Annealing of Te-Implanted GaAs by Ruby Laser Irradiation," Applied Physics Letters, 32: 147 (1978).

8. Mullins, Bill W. "Characterization of Laser Annealing of Ion Implanted GaAs and Si Using Optical Reflectivity." M.S. thesis. Wright-Patterson AFB, Ohio: Air Force Institute of Technology, December 1979. (AFIT/GEP/PH/79D-6).

9. Miyao, Masanobu, Takao Miyzaki, and Takashi Tokuyama. "Optical Reflectivity Studies of Damage in Ion Implanted Silicon," Japanese Journal of Applied Physics, 17(5): 955-56 (1978).

10. White, C.W., et al. "Redistribution of Ion Implanted Boron Induced by Pulsed Laser Annealing," Journal of the Electro Chemical Society, In-Press, 1978.

11. Khaibullin, I.B., et al. "Some Features of Laser Annealing of Implanted Silicon Layers," Radiation Effects, 36: 225 (1978).

12. Venkatesan, T.N.C. "Dose Dependence in Laser Annealing of Arsenic-Implanted Silicon," Applied Physics Letters, 33(5): 429-31 (September 1978).

13. Smith, J. Lynn. "Surface Damage of GaAs from .694 and 1.06-μm Laser Radiation," Journal of Applied Physics, 43: 3399 (1972).

14. Liu, Y.S., and K.L. Wang. "A Transient Optical Reflectivity Study of Laser Annealing of Ion-Implanted Silicon: Threshold and Kinetics," Applied Physics Letters, 34(6): 363-65 (15 March 1979).

15. Auston, D.H., et al. "Dynamics of Laser Annealing," American Institute of Physics Conference Proceedings, No. 50: 11-26 (1978).

16. Kim, Q., et al. "Laser Annealing of Ion-Implanted GaAs," American Institute of Physics Conference Proceedings, No. 50: 597-602 (1978).

17. Bradley, Kenneth R. "Laser Annealing of and Laser Interactions With Ion Implant Semiconducting Materials." M.S. thesis. Wright-Patterson AFB, Ohio: Air Force Institute of Technology, December 1979. (AFIT/GEP/PH/79D-1).

18. Campisano, S.U., et al. "Laser Pulse Annealing of Ion-Implanted GaAs," Journal of Applied Physics, 51(1): 295-98 (January 1980).

19. Sze, S.M. Physics of Semiconductor Devices. New York: John Wiley & Sons, Inc., 1969.

20. Beaglehole, D. "A Sensitive Single Beam Device for Continuous Reflectance or Transmission Measurements," Applied Optics, 7(11): 2218-20 (November 1968).

21. Wooten, Frederick. Optical Properties of Solids. New York: Academic Press, 1972.

22. McKelvey, John P. Solid State and Semiconductor Physics. New York: Harper and Row, 1976.

23. Shifrin, G.A., et al. "Effect of Ion-Implantation Damage on the Optical Reflection Spectrum of Gallium Arsenide," Applied Physics Letters, 17(7): 274-76 (October 1970).

24. Grasso, V., et al. "Optical Reflectivity of Ion-Implanted Amorphous GaAs," Applied Physics Letters, 33(7): 632-33 (October 1978).

25. Kim, Q., et al. "Characterization of Ion-Implanted GaAs by Ellipsometry," Journal of Applied Physics, 51(4): 2024-29 (April 1980).

26. Brice, D.K. "Ion Implantation Range and Energy Deposition Distributions," IFI. New York: Plenum, 1971.

27. Yen, E.T., et al. Procedures 4th Intern. Conf. Ion Implantation in Semiconductors and Other Materials, Osaka, edited by S. Namba. New York: Plenum, 1974.

Appendix A

Aluminum coated reflective surfaces can be made using various techniques and procedures which, in general, are basically the same since certain processing requirements must be fulfilled. The procedure used in this experiment consisted of a consolidation of advice and information from several sources.

The aluminum was deposited on a piece of microscopic glass slide. The thickness of the aluminum was 1000Å, and a protective coating of MgF_2 was deposited over the aluminum to a thickness of 400Å. The MgF_2 protects the aluminum from oxidation effects. All deposition was performed within a vacuum of 2×10^{-7} torr. During deposition, a radiative heater was used to maintain the glass slide at a temperature of 100°C.

The following explains in detail each stage of the making of aluminum mirrors:

Glass Surface

Standard lab grade microscopic slides, 25x75 mm, were used as the surface. A piece of glass, half-moon in shape, was cut out of the glass slide. This half-moon shaped piece must fit within the well of the sample holder of the reflectivity equipment. Cutting of the glass was performed using a sharp steel blade for the general cut of the outside circumference, and a machine shop grinding wheel to grind out the inside circumference.

Glass Surface Cleaning

The surface was cleaned using chromic acid, a mild detergent, and isopropyl alcohol. First the glass was scrubbed using cotton balls and the detergent solution. The surface was considered clean when upon removal of the glass from the solution, a thin film on the glass surface forms which does not bead, collect in areas, or recede from the edges of the glass. If this condition is fulfilled, the glass, while still wet, is placed in distilled water for rinsing. Each rinse should be performed without letting the glass surface get dry. While the glass is wet, it is transferred from the distilled water to the chromic acid and kept in the acid for five minutes. This removes organic material left on the glass by the detergent solution. After the five minutes, the glass is removed, and while still wet, placed in fresh distilled water for rinsing. After two or three rinsings, never letting the glass get dry, the glass is immersed in isopropyl alcohol.

Glass Removal from Isopropyl Alcohol

The glass must be removed from the isopropyl alcohol in such a manner that it is the alcoholic vapors which dry the glass surface and not the ambient air. This is accomplished by use of a heat air gun. Direct the heat of the air gun onto the surface of the alcohol. This will cause alcoholic vapors to form above the surface. The alcoholic vapors cannot be seen, but it is through this vapor cloud that the glass is pulled very slowly. Thus, as the glass breaks through the surface of the isopropyl alcohol, it is immediately in contact with the

warm vapors. As the glass is pulled through the warm vapors, it will be dried, and thus clean. This complete operation should be performed just prior to the placing of the glass inside the vacuum chamber.

Aluminum Deposition

The aluminum is deposited on the glass surface by use of a resistive heater block and a tungsten filament. The deposition is performed within a vacuum of $2x10^{-7}$ torrs. The glass surface is suspended at least 30 cm above the tungsten filament. At the same radial distance from the filament is placed a quartz crystal which is used to monitor the thickness of the deposition. The quartz crystal connects to a Sloan Deposit Thickness Monitor. A radiative heater is suspended above the glass surface. This heater is used to maintain a temperature of 100°C on the glass itself. Aluminum pieces, 99.99% pure, are hung on the tungsten filament just prior to evacuating the system within the vacuum chamber. A small shield is placed between the glass surface and the aluminum. It should be arranged so as to permit its repositioning after the system is under a vacuum. The purpose of the screen is to prevent initial contaminants which are within the filament and the aluminum from being deposited on the glass surface. This is accomplished by first heating the filament to a hot-orange glow while under a vacuum, and with the screen shielding the glass surface. Next, while maintaining the vacuum, remove the voltage from the filament, remove the screen so it no longer blocks the glass surface, and reapply the voltage

to the filament. The aluminum vapors will thus be deposited on the glass surface. The 1000Å thickness, monitored by the Sloan instrument, should be reached within 30 sec. This deposition rate should not be very much slower than 1500Å/minute. Upon completion of the aluminum deposition, the screen is placed back between the glass surface and now the MgF_2 while maintaining the vacuum.

MgF_2 Deposition

The procedure is the same as that of the aluminum. However, deposition is performed using an E-gun and an E-gun crucible. The MgF_2 is placed in the vacuum chamber onto the E-gun crucible at the same time as the aluminum is placed on the tungsten filament. After aluminum deposition is complete, the MgF_2, while still under the constant vacuum, is deposited to a thickness of 400Å. The screen is used to block off initial contaminants, and the radiative heater provides the heat to the MgF_2 which causes the MgF_2 to harden to a relatively dense surface overcoat.

Upon completion of both depositions, the glass surface, now coated with aluminum and MgF_2, should be placed in a container which will prevent the surface from getting scratched or contaminated.

Vita

Ricardo Antonio Contreras was born on 23 December 1947 in Los Angeles, California, the son of Richard Moses and Alice Mary Contreras. He graduated from Garfield High School in Los Angeles, California in 1966. In April 1967, he enlisted in the Air Force and was assigned to Ballistic Missile Analyst Technician School at Chanute AFB, Illinois. Upon graduation, he was assigned to the Strategic Air Command.

In June 1974, he was selected for the Airmen's Educational Commissioning Program. He was then assigned to California State University at San Diego and graduated in December 1975 with a Bachelor of Science degree in Electrical Engineering. He received his commission upon graduation from Officer Training School in April 1976. His first assignment after OTS was to the Space and Missile Test Center at Vandenberg AFB, California, where he performed his duties as a Satellite Engineer in charge of test, launch, and evaluation of space systems. In March 1979, he was assigned to the Air Force Institute of Technology.

Permanent Address: 9334 Wampler
Pico Rivera, Ca.
90660

UNCLASSIFIED

SECURITY CLASSIFICATION OF THIS PAGE (When Data Entered)

REPORT DOCUMENTATION PAGE		READ INSTRUCTIONS BEFORE COMPLETING FORM
1. REPORT NUMBER AFIT/GEO/PH/80D-5	2. GOVT ACCESSION NO. AD-A094 946	3. RECIPIENT'S CATALOG NUMBER
4. TITLE (and Subtitle) MULTIPULSE LASER ANNEALING OF SELENIUM IMPLANTED GaAs		5. TYPE OF REPORT & PERIOD COVERED MS Thesis 6. PERFORMING ORG. REPORT NUMBER
7. AUTHOR(s) Ricardo A. Contreras Captain USAF		8. CONTRACT OR GRANT NUMBER(s)
9. PERFORMING ORGANIZATION NAME AND ADDRESS Air Force Institute of Technology (AFIT/EN) Wright-Patterson AFB, Ohio 45433		10. PROGRAM ELEMENT, PROJECT, TASK AREA & WORK UNIT NUMBERS
11. CONTROLLING OFFICE NAME AND ADDRESS Avionics Laboratory/Air Force Wright Aeronautics Laboratory Wright-Patterson AFB, Ohio 45433		12. REPORT DATE 12 December 1980 13. NUMBER OF PAGES 79
14. MONITORING AGENCY NAME & ADDRESS(if different from Controlling Office)		15. SECURITY CLASS. (of this report) UNCLASSIFIED 15a. DECLASSIFICATION DOWNGRADING SCHEDULE

16. DISTRIBUTION STATEMENT (of this Report)

Approved for public release; distribution unlimited.

17. DISTRIBUTION STATEMENT (of the abstract entered in Block 20, if different from Report)

18. SUPPLEMENTARY NOTES

Approved for public release; IAW AFR 190-17

Frederick C. Lynch, Major, USAF
Director of Public Affairs

06 JAN 1981

19. KEY WORDS (Continue on reverse side if necessary and identify by block number)

Laser Annealing
Ion Implantation
Gallium Arsenide
Optical Reflectivity

20. ABSTRACT (Continue on reverse side if necessary and identify by block number)

GaAs implanted with 120 keV Se at a fluence of 10^{14} ions/cm^2 was laser annealed using .53μ energy from a Q-switched, frequency doubled, Neodymium:YAG laser. The substrates were irradiated in air by either a single pulse or multipulse with an average energy density of 300 mj/cm^2 per pulse. The pulse width (FWHM) was 15 ns. Optical reflectivity in the ultraviolet

DD FORM 1 JAN 73 1473 EDITION OF 1 NOV 65 IS OBSOLETE

UNCLASSIFIED

SECURITY CLASSIFICATION OF THIS PAGE (When Data Entered)

Block 20:

spectrum of 210 nm to 380 nm was used to evaluate the crystalline structure. The relative crystalline damage versus depth profile was obtained and compared to that of an as-implanted sample. The depth profiling was accomplished using a chemical etch. Implanted samples annealed at 1, 2, 4, 8, and 12 pulses all showed a dramatic reduction of damage as compared to the as-implanted sample. However, the results of the two pulse anneal show the highest degree of recrystallization approaching that of a virgin sample.


DATE
ILME